The Plant Cell, Vol. 24: 2792–2811, July 2012, www.plantcell.org

Downregulation of the δ-Subunit Reduces Mitochondrial ATP Synthase Levels, Alters Respiration, and Restricts Growth and Gametophyte Development in *Arabidopsis*[W][OA]

Daniela A. Geisler,[a] Carola Päpke,[a] Toshihiro Obata,[a] Adriano Nunes-Nesi,[a,b] Annemarie Matthes,[a] Kay Schneitz,[c] Eugenia Maximova,[a] Wagner L. Araújo,[a,b] Alisdair R. Fernie,[a] and Staffan Persson[a,1]

[a] Max-Planck-Institut für Molekulare Pflanzenphysiologie, D-14476 Potsdam-Golm, Germany
[b] Departamento de Biologia Vegetal, Universidade Federal de Viçosa, 36570-000 Minas Gerais, Brazil
[c] Entwicklungsbiologie der Pflanzen, Technische Universität München, 85354 Freising, Germany

The mitochondrial ATP synthase (F_1F_o complex) is an evolutionary conserved multimeric protein complex that synthesizes the main bulk of cytosolic ATP, but the regulatory mechanisms of the subunits are only poorly understood in plants. In yeast, the δ-subunit links the membrane-embedded F_o part to the matrix-facing central stalk of F_1. We used genetic interference and an inhibitor to investigate the molecular function and physiological impact of the δ-subunit in *Arabidopsis thaliana*. Delta mutants displayed both male and female gametophyte defects. RNA interference of delta resulted in growth retardation, reduced ATP synthase amounts, and increased alternative oxidase capacity and led to specific long-term increases in Ala and Gly levels. By contrast, inhibition of the complex using oligomycin triggered broad metabolic changes, affecting glycolysis and the tricarboxylic acid cycle, and led to a successive induction of transcripts for alternative respiratory pathways and for redox and biotic stress-related transcription factors. We conclude that (1) the δ-subunit is essential for male gametophyte development in *Arabidopsis*, (2) a disturbance of the ATP synthase appears to lead to an early transition phase and a long-term metabolic steady state, and (3) the observed long-term adjustments in mitochondrial metabolism are linked to reduced growth and deficiencies in gametophyte development.

INTRODUCTION

The membrane-bound F_1F_o H^+-ATP synthase in the inner mitochondrial membrane catalyzes the terminal step of oxidative phosphorylation, which converts the electrochemical proton gradient into ATP. The matrix-facing central stalk belongs to the F_1 domain and links the catalytic subunits to the membrane-embedded F_o part. Proton flow from the intermembrane space into the matrix drives the rotation of the F_o domain and the attached central stalk, and the immobilized α- and β-subunits of F_1 subsequently catalyze the synthesis of ATP (Gledhill and Walker, 2006). The ATP synthase complex (~600 kD) can also form dimers, which were first purified from yeast (Arnold et al., 1998) and also from algae (Dudkina et al., 2005). These dimers form row-like structures and are suggested to induce the curvature of the inner mitochondrial membrane (Paumard et al., 2002; Dudkina et al., 2010).

In plants, the requirement for ATP varies considerably between tissues and developmental stages. Energy demands appear to be particularly high in developing anthers, as shown by their high number of mitochondria and by the 10-fold faster respiration measured in pollen grains compared with leaf tissue (Lee and Warmke, 1979; Tadege and Kuhlemeier, 1997). Indeed, mutations in several respiratory chain proteins lead to male sterility, while the somatic growth is in many cases not visibly affected (Rasmusson et al., 1998; Hanson and Bentolila, 2004). A naturally occurring and widespread type of sterility in self-fertilizing crop species is cytoplasmic male sterility (cms), which is caused by chimeric genes in the mitochondrial genome, for example, containing parts of the ATP synthase subunit genes *Atp1*, *Atp6*, *Atp8*, and *Atp9* (Hanson and Bentolila, 2004). Fertility can be regained in many cases by expression of nuclear fertility restorer genes that interfere with the chimeric gene or protein in several ways (Hanson and Bentolila, 2004; Wang et al., 2006). One of the best studied cms mutants is *Nicotiana sylvestris* CMSII, which is deficient in the NAD7 subunit of complex I. Lack of a functional complex I leads to broad physiological adaptations and a partial male sterility that can be rescued by high light (Gutierres et al., 1997; Dutilleul et al., 2003a, 2005). Male sterility can also be caused by genetic interference of nuclear-encoded genes for respiratory proteins, such as shown for mutants in the F_Ad subunit of the ATP synthase (Li et al., 2010), the flavoprotein subunit succinate dehydrogenase 1 (SDH1) of complex II (León et al., 2007), and by antisense repression of the NADH binding (55 kD) subunit of complex I (Heiser et al., 1997). By contrast, aberrations in female tissues have not been commonly observed in respiratory mutants with the notable exception of the *sdh1-1* mutant for complex II (León et al., 2007).

The mechanisms that lead to male sterility in cms and other respiratory mutants have not been fully established. For some

[1] Address correspondence to persson@mpimp-golm.mpg.de.
The author responsible for distribution of materials integral to the findings presented in this article in accordance with the policy described in the Instructions for Authors (www.plantcell.org) is: Staffan Persson (persson@mpimp-golm.mpg.de).
[W] Online version contains Web-only data.
[OA] Open Access articles can be viewed online without a subscription.
www.plantcell.org/cgi/doi/10.1105/tpc.112.099424

cms mutants, it is known that retrograde signaling from the mitochondrion to the nucleus plays a role; however, the nature of the signal is not known (Carlsson et al., 2008). It is also unclear if changes in the ATP/ADP ratio directly contribute to sterility, since some mutants show a reduction in the ATP/ADP ratio in flower tissue (Bergman et al., 2000), whereas others do not (Teixeira et al., 2005; Busi et al., 2011). Apart from being energy requiring, pollen development is also a highly regulated process where synchrony between gametophytic and the surrounding sporophytic tissue development is crucial (Ma, 2005; Wilson and Zhang, 2009). The connection to the sporophyte and the dependence on nutrients from the surrounding tissue is even more pronounced for the female than for the male gametophyte. Unfortunately, only few studies have been performed on the vegetative or floral tissues of sterile respiratory mutants to establish the factors that could contribute to gametophyte disorders.

In animals and yeast (*Saccharomyces cerevisiae*), the δ-subunit is an essential part of the F_1 domain of the ATP synthase. Mitochondria of yeast delta null mutants and lines with repressed δ-subunit expression are unable to couple ATP synthesis to the flow of protons through F_o and are thus defective in oxidative phosphorylation (Lai-Zhang et al., 1999; Duvezin-Caubet et al., 2003). While several functional aspects of the δ-subunit are well understood in yeast, animals, and bacteria, very little is known in plants. In *Arabidopsis thaliana*, the δ-subunit is nuclear encoded and represented by a single gene (At5g47030). However, the functional role of the plant homolog is unknown. The only report on the physiological role of a plant-related δ-subunit isoform is from cotton (*Gossypium hirsutum*), in which one of three delta homologs is highly expressed in elongating fibers, a cell type with a particularly high ATP/ADP ratio (Pang et al., 2010). Our aim was to establish the molecular and physiological function of the δ-subunit of the mitochondrial ATP synthase in *Arabidopsis* and to study the effects of a disturbed ATP synthase on primary metabolism. We show that perturbing the δ-subunit affects plant growth, female and male gametophyte development, and ATP synthase amounts, accompanied by specific metabolic changes. To compare these long-term effects to an acute inhibition, we treated light-grown seedling cultures with the ATP synthase inhibitor oligomycin. We discuss possible effects of the observed metabolic and transcript changes on plant development and compare our results with published data for complex I.

RESULTS

Male Sterility and Female Defects in a Mutant for the δ-Subunit of the Mitochondrial ATP Synthase

To assess the impact of reduced transcripts for the δ-subunit on plant growth and development, we obtained T-DNA insertion lines for the delta gene (At5g47030) from the SAIL mutant collection (Sessions et al., 2002). Four lines were identified, of which three contained T-DNA inserts in the promoter region (SAIL_205_C06, SAIL_3_F04, and SAIL_346_G06), and one held an insert in the intron of At5g47030 (SAIL_755_C04; Figure 1A). The lines with T-DNA inserts in the promoter produced homozygous plants without any decrease in delta transcript as tested by quantitative RT-PCR (qRT-PCR; data not shown). By contrast, we were unable to obtain homozygous plants from the intron-located insertion line (SAIL_755_C04; *atpδ-1*). Moreover, the heterozygous *atpδ-1* plants produced ~50% deformed pollen that were unable to germinate (Figure 1B), indicating that lack of the δ-subunit is male gametophytic lethal. A detailed analysis of the pollen grains by transmission electron microscopy revealed that the pollen of the heterozygous *atpδ-1* line displayed a more diverse ultrastructure. The intine was thicker and less electron dense (Figure 1C), and the tapetum seems to have degenerated at a later stage in the mutant compared with wild type (see Supplemental Figure 1A online). Additionally, pollen grains from the mutant contained larger, more elongated mitochondria with a less condensed matrix compared with the wild type (Figure 1D; see Supplemental Figure 1B online). The pollen-deficient phenotype of *atpδ-1* was rescued by expressing the delta gene under 1 kb of its endogenous promoter. Additionally, 70% of the complemented F2 generation of *atpδ-1* plants was resistant to BASTA (which is part of the T-DNA insertion cassette) and also produced homozygous plants, whereas only 11% of the non-complemented *atpδ-1* survived (see Supplemental Table 1 online). This shows that the complemented plants produced functional delta protein and confirms that the T-DNA insert in the delta gene caused the fertility disorders in *atpδ-1*.

To determine the transmission efficiencies of the T-DNA insertion through the gametophytes, we performed reciprocal backcrosses between the heterozygous *atpδ-1* line and wild-type plants. Fertilization of the female wild type with pollen from the heterozygous *atpδ-1* line produced only wild-type plants, confirming that the T-DNA insertion could not be transmitted via mutant pollen. Fertilization of the heterozygous female mutant with wild-type pollen resulted in ≤13% heterozygous plants instead of the expected 50% for a male sterile mutant. The female transmission efficiency of the insert is thus ≤26%, suggesting that apart from an effect on the female gametophyte, the T-DNA insertion also seems to disturb the surrounding sporophyte. To investigate how disruption of the gene for the δ-subunit affected the female gametophyte, we analyzed ovules at floral stage 13 (Smyth et al., 1990). In the mutant, 77% of the ovules were still at the stage of embryo sac development compared with 27% in the wild type. Most of the wild-type ovules showed already a two-nuclear endosperm (45%) or a four-nuclear endosperm (24%), whereas only 5 and 8% of the ovules had reached these stages in the *atpδ-1* mutant, respectively (Figure 1E). This indicates that the majority of ovules in the mutant developed slower compared with those of the wild type. No major differences were observed between flowers of wild type and mutant, with the exception of brown spots visible on mutant anthers (Figure 1F). However, ~25% of the seeds within the siliques in the heterozygous *atpδ-1* mutant (n = 536 seeds of 10 plants) were shriveled and colored white or brown, indicating embryo lethality at this stage (Figure 1G).

High Expression of the Delta Gene in Pollen, Ovules, and Floral Primordia

To create a detailed expression profile for the delta gene, we conducted RNA in situ hybridizations in wild-type flowers and

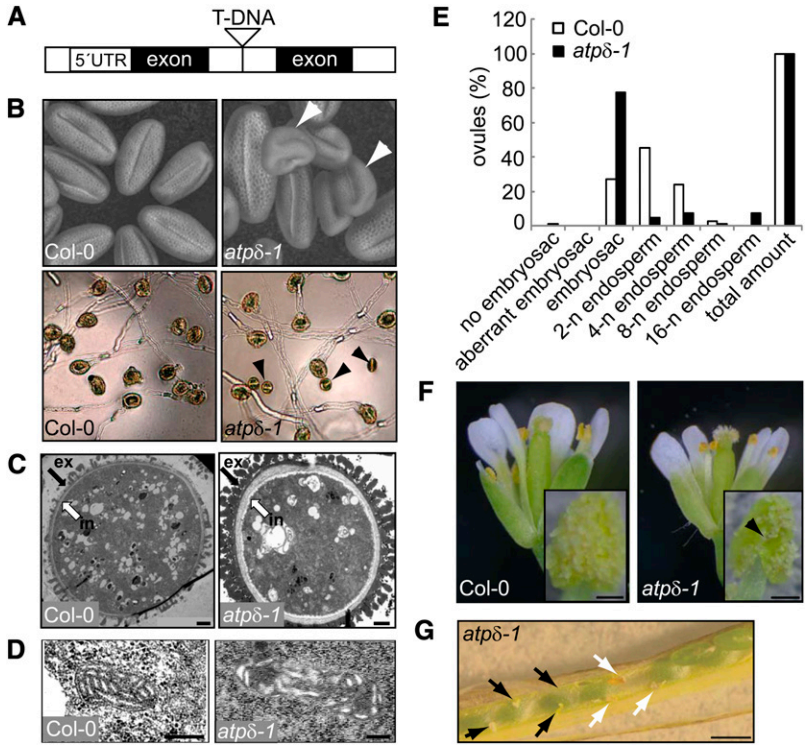

Figure 1. A Mutation in the Delta Gene Results in Male and Female Gametophyte Defects.

(A) Schematic view of the site of T-DNA insertion in SAIL_755_C04 (*atpδ-1*). UTR, untranslated region.
(B) Pollen grains from the wild type (Col-0) and *atpδ-1* imaged by environmental scanning electron microscopy (top panels) and pollen tube growth assays (bottom panels). Deformed pollen (white arrowheads; top panels) were not able to germinate (black arrowheads; bottom panels).
(C) and **(D)** Morphology of pollen grains and ultrastructure of pollen mitochondria imaged by energy filtering transmission electron microscopy in the wild type (Col-0) and *atpδ-1*.
(C) In the mutant pollen grain, both the exine (ex; black arrows) and the intine (in; white arrows) were thicker compared with wild-type pollen, with the intine appearing less electron dense. Bars = 1 μm.
(D) In wild-type pollen grains, the mitochondria were characterized by an oval shape with a condensed matrix and well-organized cristae. In mutants, the mitochondria were more elongated and showed a modest decrease in electron density in the matrix. Furthermore, the cristae were more loosely distributed and showed a slight swelling in the mutant. Bars = 250 nm.
(E) Quantitative differences in ovule development between wild type (Col-0) and *atpδ-1* at floral stage 13 (Col-0, $n = 33$; *atpδ-1*, $n = 159$). 2-n to 16-n, two-nuclear to 16-nuclear endosperm.
(F) Flowers and anthers with pollen (inset). Brown pollen are indicated by a black arrowhead. Bars = 0.5 μm.
(G) Siliques of *atpδ-1* containing abnormal seeds. White and black arrows indicate shriveled brown seeds and absent seeds, respectively. Bars = 0.5 mm.

inflorescences. We found that the delta gene is highly expressed in pollen, in the innermost anther tissue (tapetum), and in ovules (Figures 2A and 2B). The staining was particularly high in young flower buds and in floral primordia of inflorescences (Figures 2C and 2D). Flowers from plants carrying promoter fusions of delta with the β-glucuronidase (GUS) reporter gene showed expression in the anthers and pollen, as well as in stigma (Figures 2E to 2G). The high intensity of GUS staining in the older flowers can be explained by a sustained presence of GUS protein in older tissues. GUS expression in etiolated seedlings was confined to the upper part of the hypocotyl and the root (Figures 2H to 2J). Light-grown seedlings showed highest GUS staining in cotyledons and particularly guard cells (Figures 2K and 2L). We conclude that the delta gene is expressed both in gametophytic and vegetative tissues and particularly in tissues with high energy requirements.

Growth Retardation, Deformed Pollen, and Reduced Amounts of Assembled F_1F_o Complex in Plants with Downregulated δ-Subunit

The ubiquitous expression of the delta gene suggests that it has important functions also in other tissues and organs than the male and female gametophytes. To obtain information about this, we placed 267 bp of the delta cDNA in sense and antisense direction under a dexamethasone (Dex)-inducible promoter using the pV-TOP system (Craft et al., 2005; Figure 3A). Off-target effects of RNA interference (RNAi) constructs in plants have been suggested for fragments of 21 to 24 nucleotides or more (Watson et al., 2005; Rossel et al., 2007). Additionally, it has been computationally predicted that between 50 to 70% of gene transcripts in plants have potential off-targets when used for posttranscriptional gene silencing (Xu et al., 2006). We therefore decided to confirm that nonspecific gene silencing had not

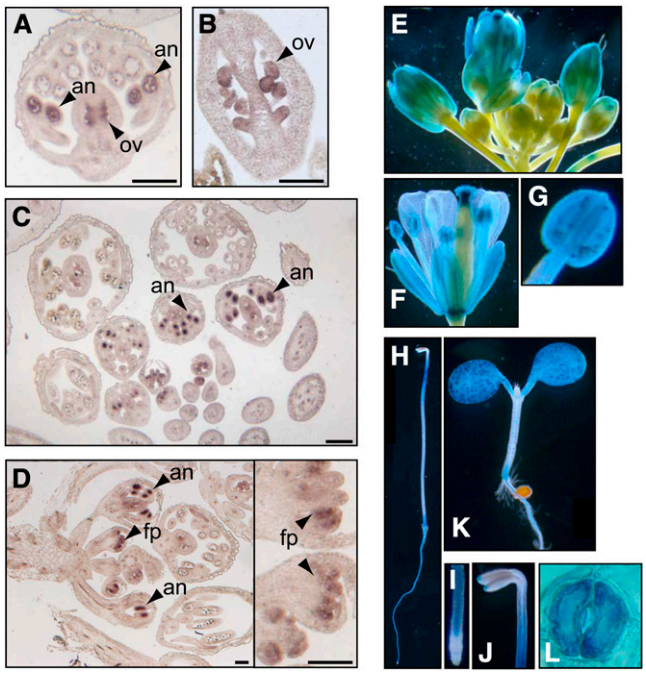

Figure 2. Expression of Delta Transcripts in Gametophytic and Vegetative Tissues.

(A) to **(D)** RNA in situ hybridizations with delta antisense probes. Transverse (**[A]** and **[C]**) and longitudinal (**[B]** and **[D]**) sections through wild-type inflorescences. Arrowheads mark highly stained tissues. an, anthers; fp, floral primordia; ov, ovules. Bars = 100 μm.

(E) to **(L)** Plants and seedlings carrying delta promoter fusions with the GUS reporter gene.

(E) to **(G)** Inflorescence, flower, and anther of soil-grown plants.

(H) to **(J)** Seven-day-old etiolated seedling **(H)** with close-ups of the root tip **(I)** and cotyledons **(J)**.

(K) and **(L)** Seven-day-old light-grown seedling **(K)** with high GUS expression in stomata **(L)**.

taken place in our studies. The fragment used for the RNAi construct was designed to have minimal complementarity with other genes; thus, a BLAST query against the whole *Arabidopsis* genome or Arabidopsis Genome Initiative transcripts (www.Arabidopsis.org) revealed the absence of identical regions of around 20 nucleotides. It can therefore be anticipated that there were no regions of identity to any other transcript that could potentially be responsible for the phenotypes observed here.

Transformation of *Arabidopsis* plants with the inducible delta RNA interference (δRNAi) construct yielded six independent transgenic lines with strong specific GUS reporter activity in Dex-treated leaves (a GUS cassette is also activated in pV-TOP by the treatment and is therefore suitable for screening purposes; Craft et al., 2005). Three of the lines (δRNAi1, δRNAi2, and δRNAi3) showed a strong decrease in transcript for the δ-subunit after induction with 20 μM Dex in leaves of the F2 generation (Figure 3B) and were thus characterized further in the F3 generation. Two of the three δRNAi lines showed severe growth retardation compared with controls when grown on agar supplemented with 50 μM Dex (Figure 3C). To assess whether downregulation of delta transcripts can mimic the pollen deficiency of *atpδ-1*, δRNAi lines were grown on soil and watered with a solution of 50 μM Dex or DMSO (as solvent control) for 2 weeks. δRNAi1 and δRNAi2 showed growth delays and additionally produced deformed pollen (Figure 3D). The absence of pollen deficiency in δRNAi3 could be due to the weaker reduction of delta transcript seen after qRT-PCR (Figure 3B), which could have resulted in a higher basal expression of the delta gene in those plants than in δRNAi1 and δRNAi2 lines.

In yeast, the δ-subunit is essential for the function of the ATP synthase. In delta-deficient yeast mitochondria, several subpopulations of the F_1F_o complex, including very low amounts of the fully assembled F_1F_o, were visible after blue native PAGE (BN-PAGE) (Duvezin-Caubet et al., 2003). δ-Subunit deficiency also leads to severe growth defects on nonfermentable media. To determine whether a decrease in delta transcript is also reducing the F_1F_o complex in *Arabidopsis*, we grew δRNAi1 and the empty vector control seedlings in liquid cultures supplemented with 30 mM Suc and 100 μM Dex for 2 weeks. Delta transcripts were strongly reduced in the δRNAi1 liquid cultures compared with the controls as shown by qRT-PCR (see Supplemental Figure 2A online). To investigate the assembly of the F_1F_o complex, we performed BN-PAGE on mitochondria purified from the 2-week-old cultures. The overall band pattern on the Coomassie blue–stained gels looked similar for δRNAi1 and the empty vector control line with respect to the amount and sizes of supercomplexes I+III, complex I, complex III, and the F_1 part of the ATP synthase (Figure 4A). However, the band corresponding to the F_1F_o complex was specifically decreased in δRNAi1 lines. These results indicate that the δ-subunit is important for the stability and/or assembly of the ATP synthase. The absence of specific antibodies against the *Arabidopsis* δ-subunit prompted us to perform SDS-PAGE analyses of the BN gel in the second dimension to investigate if the delta protein was present in the F_1F_o complex. The spot pattern of the F_1F_o complex looks similar in δRNAi1 and the control (Figures 4B and 4C). The δ-subunit protein was detected in the spots from the F_1F_o complex of both control and RNAi samples by liquid chromatography–mass spectrometry analyses (see Supplemental Data Set 1 online). This confirms that the δ-subunit is present in the F_1F_o complex of mitochondria from the induced δRNAi1 line. The decrease in F_1F_o complex amounts in δRNAi1 seedlings with reduced delta transcripts indicates that, similar to the situation in yeast, the δ-subunit is of structural importance for the ATP synthase in *Arabidopsis.*

Growth, Respiratory Parameters, and Metabolite Profiles after Downregulation of the δ-Subunit

To assess the physiological implications of a reduction in mitochondrial ATP synthase, we germinated the δRNAi and the control lines on Murashige and Skoog (MS) plates supplemented with Dex or DMSO (control). We then grew the seedlings under long-day, short-day, and dark conditions. We observed strong growth retardation of the induced δRNAi lines under long-day conditions, with leaf expansion being strongly affected (Figures 5A and 5B; see Supplemental Figure 3A online), whereas under short-day conditions, the phenotypic differences between the lines were less drastic (see Supplemental Figures 3B and 3C

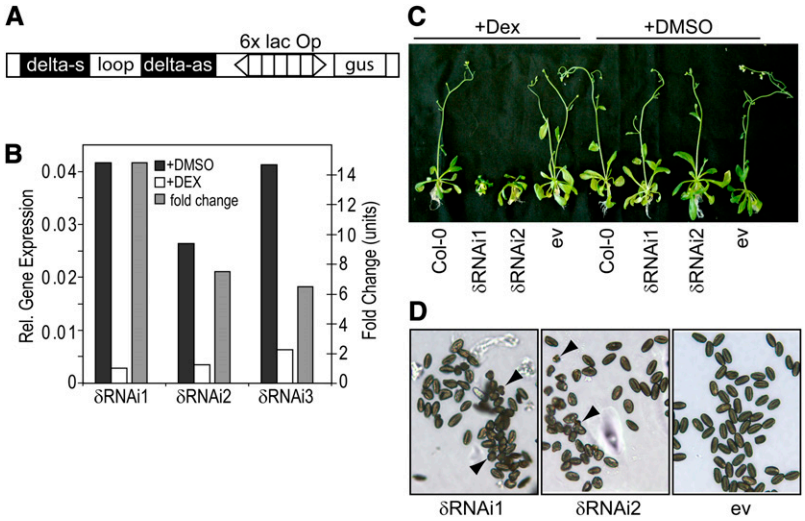

Figure 3. RNA Interference of the δ-Subunit Gene in a Dex-Inducible System Affects Plant Growth and Pollen Development.

(A) Schematic outline of the inducible RNAi pV-TOP construct. delta-s, 1 to 267 bp of the delta cDNA sequence in sense direction; delta-as, same part of the delta sequence in antisense direction; loop, sense and antisense sequences are separated by the first intron of GA 20-oxidase; lac op, lac operon.
(B) δ-Subunit expression levels relative to transcripts for glyceraldehyde-3-phosphate dehydrogenase and the calculated fold change of delta transcripts in leaves of three independent transformants carrying the RNAi construct (δRNAi1, δRNAi2, and δRNAi3) after treatment with either 20 μM Dex or DMSO (solvent control) for 24 h. The left primer was designed to bind just upstream of the start of the intron (at 249 bp) and the right primer at 105 bp downstream of the intron (at 388 bp).
(C) Phenotypes of two independent δRNAi lines grown on agar supplemented with 30 mM Suc and 50 μM Dex or DMSO for four weeks. δRNAi1 and δRNAi2 are denoted as in **(B)**; Col-0, wild type; ev, empty pV-TOP vector.
(D) Pollen phenotype of plants watered with 50 μM Dex for 3 weeks. Deformed pollen is indicated by black arrowheads. Samples are denoted as in **(C)**.

online). Such variations in growth performance could be exacerbated during the relatively fast growth of plants in long-day conditions. Interestingly, no growth delays were visible in etiolated seedlings (see Supplemental Figures 3D and 3E online). However, after transfer of these seedlings to light, the expanding hypocotyls and emerging leaves were again delayed in growth in the induced δRNAi lines (see Supplemental Figure 3D online).

We next investigated if the observed growth retardations are linked to changes in respiration and in the cellular ATP/ADP ratio. The δRNAi lines were grown for 10 d on MS plates in long-day condition, supplemented with 50 μM Dex or DMSO (control) and 30 mM Suc. Leaves of these seedlings were cut and transferred to an O_2 electrode to measure total respiration rates and the capacity of the alternative oxidase (AOX) as cyanide-resistant respiration in the dark. While total respiration was similar between different lines and treatments, AOX capacity was significantly increased in two of three induced δRNAi lines compared with controls (Figures 5C and 5D). An increased AOX capacity was also observed in flower buds of soil-grown δRNAi plants watered with Dex for 2 weeks as well as in seedlings grown on Dex plates without Suc (see Supplemental Figures 4A and 4B online). Altogether, these results indicate that the respiratory chain protein setup was altered in plants with reduced levels of delta transcript.

Next, we analyzed if the increase in AOX capacity in the δRNAi lines has consequences for the cellular ATP/ADP ratio. For that, we harvested green tissue from seedlings grown on plates at the end of the night when cellular ATP is mainly derived from mitochondria and measured ATP and ADP by HPLC. Despite a tendency toward higher levels of adenylates in the induced RNAi lines, the absolute concentrations of both adenylates were not significantly different between the δRNAi lines and controls (Figure 5E), resulting in an unchanged ratio of ATP/ADP (Figure 5F). Similar results were also obtained for seedlings grown in liquid culture that were used for BN-PAGE (see Supplemental Figures 2B and 2C online). To investigate if the unchanged ATP/ADP ratio is due to long-term adjustments of the adenylate status in δRNAi lines, we measured adenylates also in seedlings treated with Dex or DMSO for a maximum of 48 h. This was done both on plates, with and without Suc, and after painting the leaves of soil-grown plants with Dex or DMSO, when delta transcript is known to be downregulated. However, no change in the ATP/ADP was observed after 1 or 2 d of treatment (see Supplemental Figures 2D and 2E online). Thus, plants with decreased delta transcript are impaired in growth under long-day conditions, while maintaining their cellular ATP/ADP ratio. These plants held up to a fourfold higher capacity of AOX, which indicates that considerable changes in mitochondrial metabolism have taken place.

To detect possible changes in metabolism that could underpin the observed growth impairment, we analyzed the abundance of major primary metabolites using an established gas chromatography–mass spectrometry (GC-MS) protocol (Lisec et al., 2006). Green tissue from 2-week-old δRNAi1, δRNAi2, and vector-control seedlings grown on MS plates supplemented with Suc and either Dex or DMSO (control) were harvested at the end of the night and

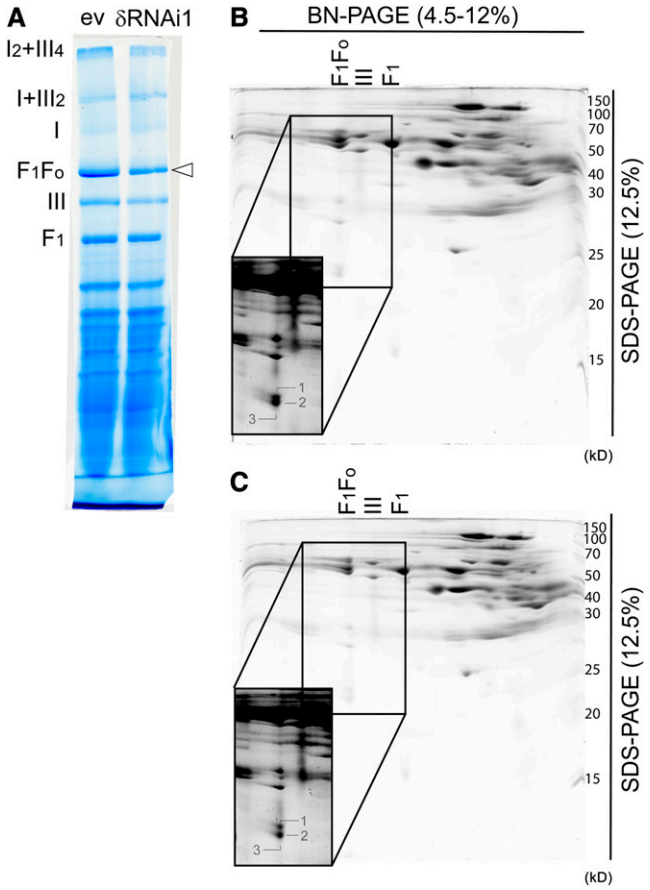

Figure 4. Reduction in Transcript for the δ-Subunit Leads to Lower Levels of Assembled F_1F_o Complex as Assessed by BN-PAGE and BN/SDS-PAGE.

Analyses of mitochondrial protein purified from *Arabidopsis* seedling liquid cultures with different expression of delta transcript using BN-PAGE and BN/SDS-PAGE. Seedlings were grown in half-strength MS medium supplemented with 30 mM Suc and 100 μM Dex for 2 weeks at 16 h light and 60 rpm. **(A)** BN-PAGE was performed with 500 μg of mitochondrial protein treated with digitonin to solubilize membranes, and the gel was stained with Coomassie blue. The gradient of the gels was 4.5 to 12%. I, complex I; F_1F_o, F_1F_o complex; III, complex III; F_1, F_1 part of F_1F_o complex; I_2+III_4 and I+III_2 denote supercomplexes of complex I and complex III in different stoichiometries. Gels from one representative experiment out of two are shown. Arrowhead indicates decrease in band intensity corresponding to the F_1F_o complex. Samples are denoted as for Figure 3.
(B) and **(C)** Two-dimensional BN/SDS-PAGE analyses of the samples shown in **(A)** for the empty pV-TOP vector **(B)** and δRNAi1 **(C)**. Lanes are denoted as in **(A)**. The positions of molecular mass markers are indicated on the right. The inset shows separated proteins of the F_1F_o complex at higher contrast. Spots 1, 2, and 3 from each gel were analyzed by liquid chromatography–mass spectrometry. The identification of the proteins for the different spots is shown in Supplemental Data Set 1 online.

used for further analyses. An about fourfold increased accumulation of Gly was observed in both Dex-induced δRNAi lines (Figure 6A). Other amino acids that showed significant increases ($P < 0.05$) were Ala, Gln, and Ser. Similar results were obtained from seedlings grown under short-day conditions with additional increases in γ-aminobutyric acid (GABA), Arg, Orn, and Lys (Figure 6B). In summary, the metabolite results suggest that a decrease in delta transcript caused specific long-term changes in mitochondrial metabolism (see Supplemental Data Set 2 online).

Metabolic Consequences of Oligomycin Inhibition of the ATP Synthase

We next investigated if the metabolite changes measured for the δRNAi lines can be elicited already by a short-term inhibition of the ATP synthase. For this, we chose oligomycin, an inhibitor which is specific for the mitochondrial ATP synthase at low concentrations (range from 0.125 to 25 μM; Krömer et al., 1988). To globally assess the impact of low levels of oligomycin, *Arabidopsis* seedlings were cultivated in liquid cultures supplemented with 30 mM Suc, which is readily taken up by the plants and converted to starch and free hexoses (Lunn et al., 2006). After 9 d under long-day conditions, the cultures were changed to fresh medium and then grown in dark for 24 h to reduce photosynthate accumulation. Oligomycin (10 μM) or the solvent control (ethanol) were added while the cultures were continuously kept in the dark (Figure 7A). We then sampled the seedlings at different time points and measured adenylates and primary metabolites. Already at the first time point at 20 min the ATP/ADP ratio started to decrease, showing that oligomycin

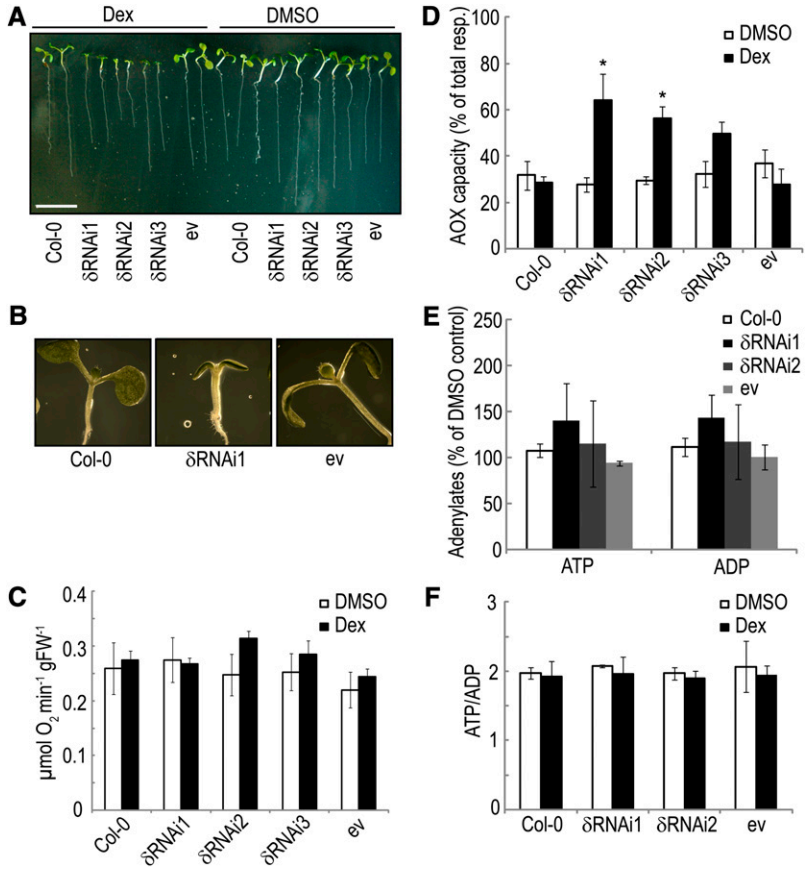

Figure 5. Increased Alternative Oxidative Capacity and Unchanged ATP/ADP Ratio after Reduction in Transcript for the δ-Subunit.

(A) The δRNAi lines and the controls were grown on MS plates supplemented with 30 mM Suc and 50 µM Dex or DMSO (control) for 10 d. Plant lines are denoted as for Figure 3. ev, empty vector control.

(B) Close-up of Dex-grown plants shown in **(A)**.

(C) Plants were grown as in **(A)** and leaves were cut and transferred directly to an O_2 electrode for measurement of total respiration as O_2 consumption in MS medium including 30 mM Suc at 25°C in the dark. Values are presented as mean ± SE of three independent experiments with two to four biological replicates each. FW, fresh weight.

(D) AOX capacity was determined after addition of KCN to inhibit complex IV and corrected for the small residual rate after addition of *n*-propyl gallate to inhibit AOX. Values are presented as in **(C)**. Asterisks indicate values that were determined by the *t* test to be significantly different ($P < 0.05$) from the Dex-treated empty vector control.

(E) ATP and ADP concentrations in leaf extracts from ~20 pooled seedlings of δRNAi lines and controls grown as in **(A)** and sampled at the end of the night. Data were normalized to the DMSO controls for each line. Values are presented as mean ± SD of two independent experiments with three plates per treatment.

(F) ATP/ADP ratios from data shown in **(E)**.

was taken up efficiently by the seedlings. After 1 h, the ATP/ADP ratio was lowered from 2.5 to 1.2 in the inhibitor-treated samples and remained at low levels until the last time point at 4 h, while control levels remained unchanged (Figure 7B). Additionally, UDP-Glc dropped slowly to about half the concentration at 4 h after oligomycin addition (Figure 7C).

Metabolite profiling was performed by GC-MS for time points 0, 1, 2, 4, and 6 h after start of treatments, and the results are presented as heat map in Figure 7D. A second independent experiment was done for time points 0, 1, and 4 h (see Supplemental Figure 5 online). Statistically significant changes ($P < 0.05$) that were seen in both experiments were layered onto the metabolic pathways shown in Figure 8. While most sugars decreased or remained unchanged, maltose levels accumulated more than fourfold in oligomycin-treated seedlings. Oligomycin treatment further led to elevated levels of glycolytic and fermentative end products, such as pyruvate, lactate, Ala, and the linked metabolites GABA and γ-hydroxybutyric acid (Figure 8; see Supplemental Data Set 2 online). By contrast, several tricarboxylic acid (TCA) cycle intermediates, such as citrate and succinate, and TCA cycle–derived amino acids (Asp, Asn, and Gln) decreased already after 1 h with the exception of fumarate, which showed a strong increase. Taken together, the results indicate a high glycolytic activity and/or a lower activity for some TCA cycle reactions.

To investigate the activity of the TCA cycle, we conducted ^{14}C-Glc feeding experiments in liquid cultures by supplying differently labeled Glc molecules. CO_2 is released from C1-labeled

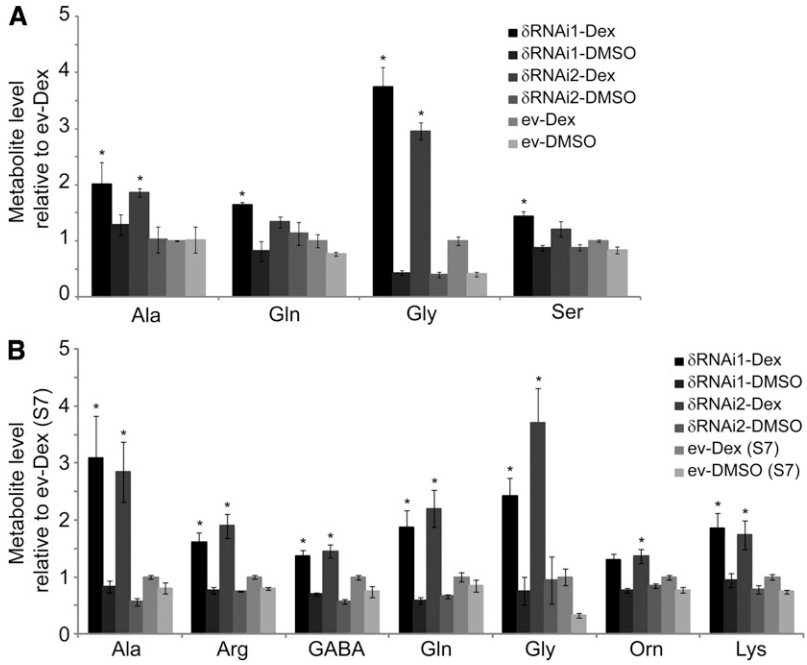

Figure 6. Reduction in Transcript for the δ-Subunit Leads to Specific Metabolic Changes.

Relative metabolite content in green tissue from induced δRNAi1 and empty vector seedlings grown on Dex or DMSO for 14 d under long- **(A)** and short-day **(B)** conditions. Data are normalized with respect to the mean response calculated for the empty vector (ev) seedlings grown on Dex. Values are presented as mean ± SE of six replicates each containing ~10 pooled seedlings. Asterisks indicate values that were determined by the *t* test to be significantly increased ($P < 0.05$) compared with the control.

Glc by the action of enzymes from nonrespiratory processes, whereas CO_2 release from C3:4 is specific to TCA cycle enzymes (Nunes-Nesi et al., 2005). A strong and significant decrease ($P < 0.05$) was observed for the TCA-related C3:4 labeled Glc in oligomycin-treated seedlings compared with controls (Figure 7E). C1-derived CO_2 release also was significantly reduced, suggesting that nonrespiratory processes were also affected by oligomycin. The ratio of $^{14}CO_2$ evolution from C3:4 to C1 provides an estimate for the relative rate of the TCA cycle compared with other processes. As shown in Figure 7F, the estimated relative TCA cycle activity was significantly lower ($P < 0.05$) in oligomycin-treated seedlings during the first 3 h of treatment. Taken together, the metabolite analyses and the Glc labeling experiments indicate that most TCA cycle reactions were substantially slower after oligomycin treatment.

Oligomycin Induces Genes for Biotic and Oxidative Stress Responses

To assess how an inhibition of the ATP synthase affects transcriptional programming and to identify potential candidates of the signaling machinery involved in ATP synthase deficiency responses, we performed transcript profiling on the same seedling liquid cultures used for metabolite profiling at time points 0, 1, and 4 h after the start of oligomycin and control treatments. The Affymetrix microarray data suggest a wide impact of oligomycin on signaling and redox-related processes. Already 1 h after addition of oligomycin a total of 102 genes was more than threefold upregulated and 14 genes were repressed, with most of them showing persistent changes (Figure 9A). Visualization of those genes by PageMan (http://mapman.mpimp-golm.mpg.de/pageman; Usadel et al., 2009) shows that the bins for mitochondrial electron transport and hormone metabolism were significantly increased (Figure 9B). After 4 h, 580 additional genes were more than threefold upregulated, and 152 genes were repressed by oligomycin. Several genes for alternative NAD(P)H dehydrogenases and AOXs (*AOX1a*, *AOX1d*, and *NDA1*) were upregulated early, and additional homologs (*NDA2*, *NDB2*, *NDB4*, and *AOX1b*) followed 4 h after the start of treatment (Figure 9C, Table 1). Additionally, several genes for complex I, complex IV, and the ATP synthase were induced, whereas hardly any genes encoding enzymes of glycolysis and the TCA cycle changed (see Supplemental Table 2 online).

Recently, a meta-analysis of microarray data sets in response to several mitochondrial dysfunctions was presented, including treatments with oligomycin and the complex I inhibitor rotenone (Schwarzländer et al., 2012). Hierarchical clustering revealed a set of marker genes for mitochondrial dysfunction, and several of those were among the highest upregulated genes in this study, such as At4g37370 (*CYP81D8*), and At5g40690 and At2g41730, which code for unknown proteins (Table 1). The only marker gene that showed a strong downregulation in response to various mitochondrial dysfunctions was the tonoplast intrinsic protein TIP2;2 (At4g17340), which was also downregulated in our study. Additionally, four of five hallmark genes for oxidative

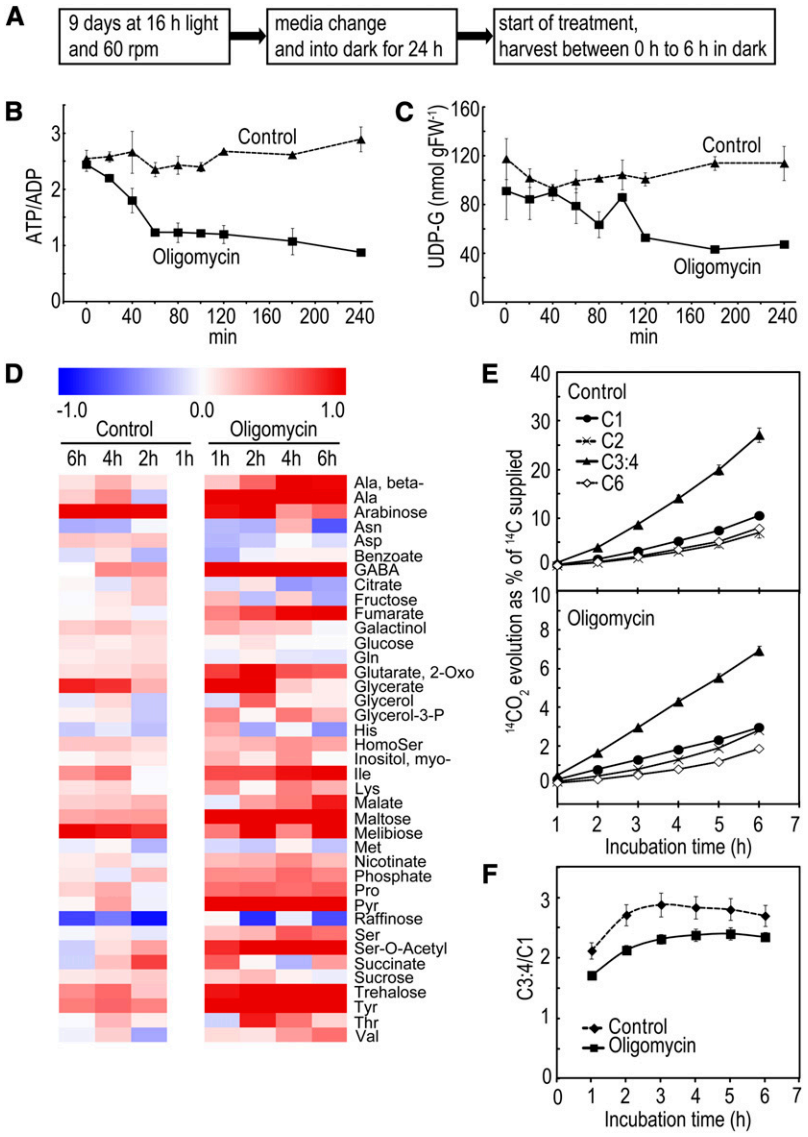

Figure 7. Inhibition of the ATP Synthase Affects Respiratory Parameters and Primary Metabolites.

(A) Experimental setup for the oligomycin treatment.

(B) and **(C)** ATP/ADP ratios **(B)** and UDP-Glc (UDP-G) **(C)** amounts in extracts of seedlings grown as in **(A)**. Values are presented as mean ± SD of two biological replicates (i.e., culture flasks). One representative experiment out of two is shown. The second experiment is presented in Supplemental Figure 5 online. FW, fresh weight.

(D) Heat map showing changes of primary metabolites in response to oligomycin treatment as in **(A)**. Data for the second independent experiment are shown in Supplemental Figure 5 online.

(E) $^{14}CO_2$ evolution from seedling cultures grown as in **(A)**. Seedlings were incubated in 10 mM MES-KOH, pH 6.5, supplemented with [1-^{14}C]-, [2-^{14}C]-, [3:4-^{14}C]-, or [6-^{14}C]Glc (at an activity concentration of 2.32 KBq mL^{-1} and specific activity of 58, 55, 54, and 56 mC$_i$ mmol^{-1}, respectively). The $^{14}CO_2$ liberated was captured in a KOH trap, and the amount of radiolabel released was subsequently quantified by liquid scintillation counting. Values are presented as mean ± SE of determinations on four individual cultures per treatment. Note that the scale on the *y* axis is different in the plots for the inhibitor treatment and the control.

(F) The ratio of $^{14}CO_2$ evolution from C3:4 to C1 positions indicates the relative rate of the TCA cycle with respect to other processes of carbohydrate oxidation. The values at 1, 2, and 3 h were determined by the *t* test to be significantly different ($P < 0.05$) from the control.

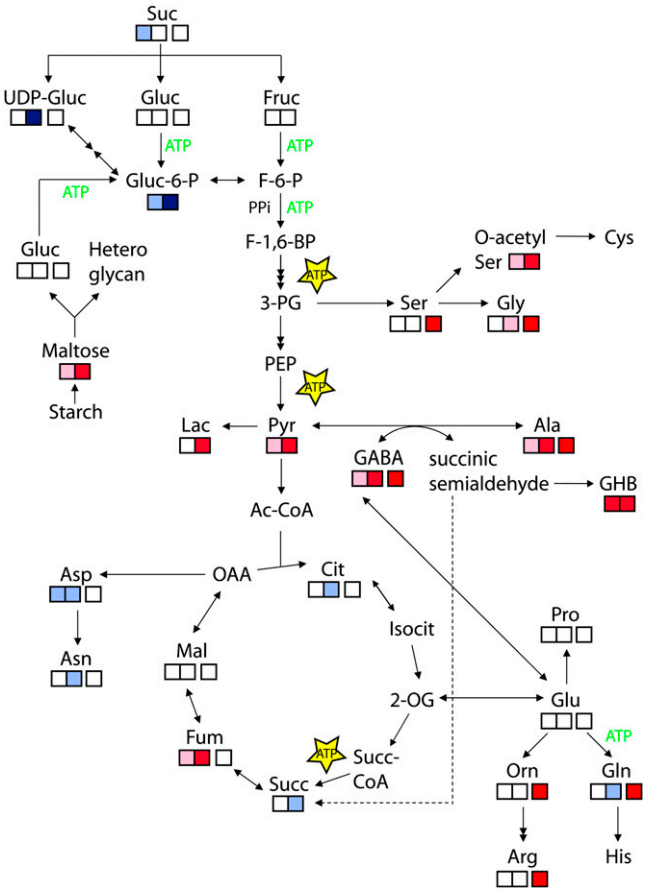

Figure 8. Cartoon of Metabolite Changes in Response to Oligomycin Inhibition of the ATP Synthase and of Lines with Downregulated δ-Subunit Expression.

The data from Figures 6, 7C, and 7D, and Supplemental Figure 5 online were layered onto a metabolic pathway cartoon and statistically significant changes in metabolite abundance compared with controls are shown by colors. For oligomycin, changes in metabolites are indicated by two adjacent squares (first square, 1 h; second square, 4 h). An increase is denoted red (pink, increase < twofold; red, increase > twofold), and a decrease is denoted blue (light blue, decrease > 0.5; dark blue, decrease < 0.5). For δRNAi1, significant increases compared with the empty vector line are indicated as separate red boxes. Empty boxes indicate no change. Gluc, Glc; UDP-gluc, UDP-Glc; Gluc-6-P, Glc-6-phosphate; F-6-P, Fru-6-phosphate; F-1,6-BP, Fru-1,6-bisphosphate; 3-PG, 3-phosphoglycerate; PEP, phospho*enol*pyruvate; Lac, lactate; Pyr, pyruvate; GHB, γ-hydroxybutyric acid; Ac-CoA, acetyl CoA; Cit, citrate; Isocit, isocitrate; 2-OG, 2-oxoglutarate; Succ-CoA, succinyl CoA; Succ, succinate; Fum, fumarate; Mal, malate; OAA, oxaloacetate; ATP in yellow symbol indicates ATP produced by the reaction; ATP in green denotes ATP consumed by the reaction. Solid arrows indicate enzymatic reactions; dashed arrow indicates the GABA shunt.

stress (Gadjev et al., 2006) were increased by oligomycin. These genes are At2g21640 (*UPOX*; Sweetlove et al., 2002), At1g19020, At1g05340, and At1g57630 and code for proteins of unknown function (see Supplemental Table 2 online). Among oxidative stress proteins with known functions, several hydrogen peroxide–responsive glutathione *S*-transferases (Kovtun et al., 2000) and *BCS1* (for *CYTOCHROME BC1 SYNTHESIS*) were strongly upregulated already after 1 h (Table 1; see Supplemental Table 2 online). *BCS1* is induced by salicylic acid and independent of other reactive oxygen signaling (ROS) pathways, such as hydrogen peroxide (Ho et al., 2008). The results indicate that several different ROS and defense signaling pathways were induced simultaneously by oligomycin. This is further corroborated by induction of several transcription factors of the WRKY and NAC families (see Supplemental Table 2 online), which have been previously implicated in coordinating cellular defense signaling (Eulgem and Somssich, 2007).

DISCUSSION

Fertility Is Decreased upon Disturbance of the ATP Synthase and Associated Alterations in Primary Metabolism

Disruption of the delta gene of the ATP synthase by a T-DNA insertion in the *atpδ-1* mutant resulted in male sterility and in defects during development of the female gametophyte. Male sterility is observed frequently upon genetic interference of nuclear-encoded respiratory genes (Heiser et al., 1997; León et al., 2007; Li et al., 2010; Busi et al., 2011), whereas aberrations in female tissues have not been commonly reported for respiratory mutants. In a mutant for SDH1 of complex II, backcrossing of mutant and wild-type plants resulted in a transmission efficiency of 60% of the T-DNA insert via the female (León et al., 2007). This partial impairment of the female gametophyte in *sdh1-1*, which is shown by defective embryo development, is suggested to be due to either an uneven distribution of functional mitochondria from the megaspore during mitosis or varying levels of nutrients coming from the tissue surrounding the ovule (León et al., 2007). In our study, the female transmission efficiency of the insert was ≤26%, suggesting that in addition to defects in embryo development (Figure 1), the female sporophyte was also affected by the mutation. Even more severe aberrations in female tissues have been reported for antisense lines of citrate synthase in potato (*Solanum tuberosum*), where a low activity of the enzyme resulted in deformed flowers and early disintegration of the ovaries (Landschütze et al., 1995), indicating that changes in primary metabolites can directly affect fertility.

In this study, we analyzed respiratory parameters and the metabolite status of plants with downregulated δ-subunit of the mitochondrial ATP synthase. The induced δRNAi plants contained lower amounts of ATP synthase than the control, showed retarded growth, and exhibited pollen deficiency, thus phenocopying the male sterility seen in *atpδ-1* mutants (Figures 3 and 4). We also determined respiratory properties of green tissues and flowers of δRNAi lines. In both cases, a dramatic increase in AOX capacity was measured in the induced lines, while the total respiration was not affected (Figure 5; see Supplemental Figure 4 online). Interestingly, an increased capacity for AOX was also observed for the complex I mutant CMSII (Dutilleul et al., 2003b). Electron transport via the non-proton-pumping AOX competes with the proton pumping cytochrome path of O_2 reduction (consisting of complex III and complex IV) and can thus bypass two of three proton pumping sites in the respiratory chain

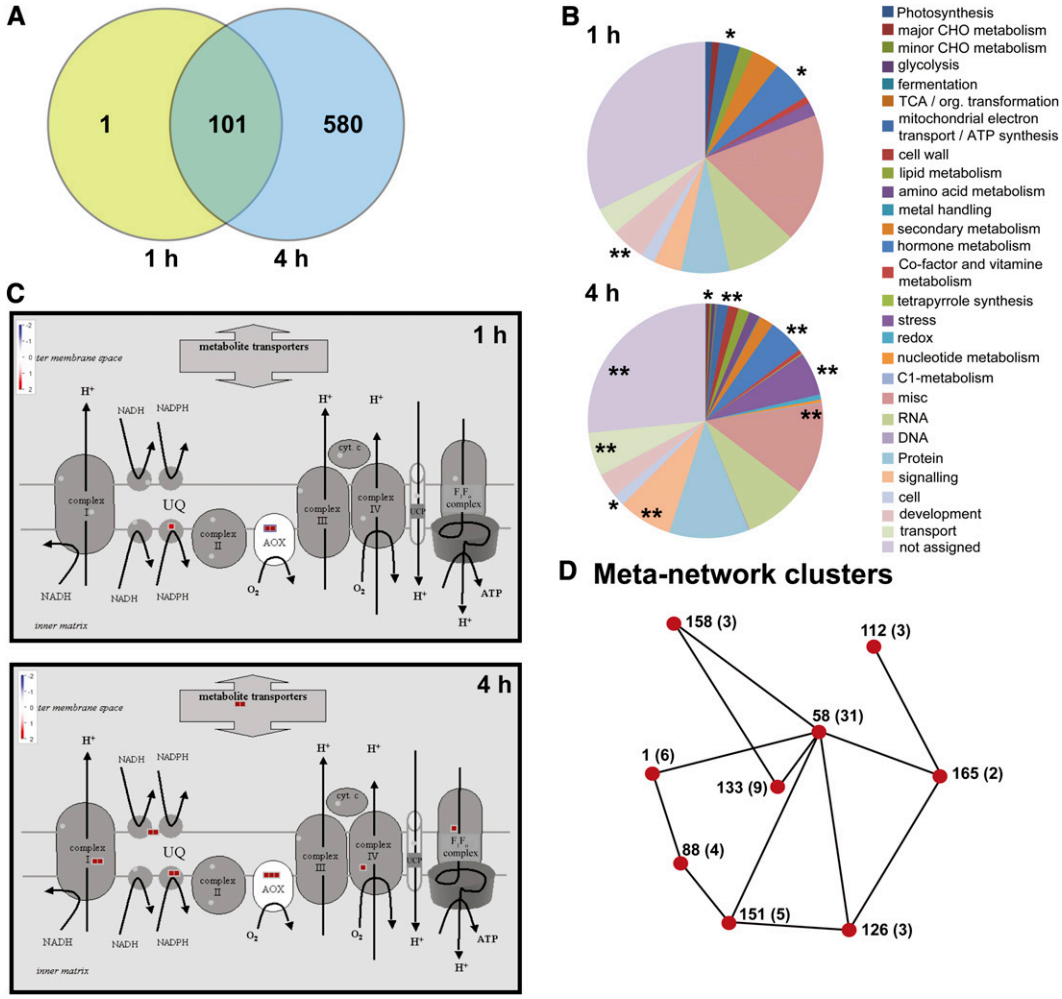

Figure 9. Inhibition of the ATP Synthase Causes Major Transcriptional Changes.

Transcriptome analyses of oligomycin-treated seedlings.

(A) Venn diagrams of comparisons of transcripts showing more than threefold upregulation between treatments of 1 and 4 h.

(B) PageMan classification of genes altered in their expression based on their MapMan ontology term allocation. Classification was done for the upregulated transcripts. One and two asterisks denote significantly overrepresented bins according to the PageMan score at $P < 0.05$ and $P < 0.01$, respectively (http://mapman.mpimp-golm.mpg.de/pageman).

(C) MapMan scheme of genes for the mitochondrial electron transport chain. Red indicates transcript increase.

(D) Meta-network of clusters in which upregulated genes are overrepresented (http://aranet.mpimp-golm.mpg.de/aranet/AraGenNet). Numbers denote cluster IDs, and the number of genes present are given in parentheses. The two most enriched MapMan terms in the different clusters are as follows: cluster 1, biotic stress and signaling; cluster 58, regulation of transcription and signaling; cluster 88, biotic stress and signaling; cluster 112, miscellaneous and hormone metabolism; cluster 126, signaling and WRKY domain transcription factor family; cluster 133, miscellaneous and transport; cluster 151, signaling and posttranslational modification; cluster 158, signaling and transport; cluster 165, signaling and stress.

(Vanlerberghe and McIntosh, 1997). It is known that the proton pumping respiratory complexes can become thermodynamically restricted and in case of complex I possibly even run in reverse direction, if the ubiquinone pool is highly reduced (Rasmusson et al., 2008). Possible consequences of such an inhibition are a decreased capacity for reoxidation of reductant, such as NADH and NADPH, and an increased production of ROS. Fewer ATP synthases in the inner membrane could in theory favor an elevated proton gradient in absence of any regulatory mechanism to decrease the proton motive force. An established function of an active AOX is to decrease the reduction state of the respiratory chain, thereby preventing excessive production of ROS (Maxwell et al., 1999; Møller and Sweetlove, 2010). A redox-balancing role of the AOX was also suggested during ammonium nutrition when the cellular reduction state is increased (Escobar et al., 2006). Thus, the increased capacity of the AOX in this study may signify attempts to dissipate reducing equivalents generated when ATP synthase amounts are decreased.

The long-term disturbance of the ATP synthase resulted in higher contents of Gly and Ala in green tissues of induced δRNAi

Table 1. Selected Transcripts Induced by Oligomycin after 1 h (or Specifically after 4 h) Grouped into Functional Classes

Class	AGI	Enzyme Description	1 h	4 h	Metabolic Process
Respiration fermentation	at3g22370	AOX1A	3.1	3.6	MET
	at1g32350	AOX1D	2.4	7.6	MET
	at1g07180	NDA1, alternative NAD(P)H Dehydrogenase 1	1.7	4.1	MET
	at4g17260	L-lactate dehydrogenase, putative	1.3	2.9	Fermentation, LDH
	at2g29990	NDA2, ALTERNATIVE NAD(P)H DEHYDROGENASE2	0.1	1.9*	MET
	at4g05020	NDB2, NAD(P)H dehydrogenase B2	0.8	2.9*	MET
	at2g20800	NDB4, NAD(P)H dehydrogenase B4; NADH dehydrogenase	0.6	2.4*	MET
	at3g22360	AOX1B	0.3	3.4*	MET
	atmg00270	NAD6, NADH dehydrogenase subunit 6	0.2	2.3*	MET
	atmg00060	NAD5, mitochondrial NADH dehydrogenase subunit 5	0.4	2.0*	MET
	atmg00650	NAD4L, encodes NADH dehydrogenase subunit 4L	0.6	1.5*	MET
	atmg00070	NAD9, NADH dehydrogenase subunit 9	0.4	1.4*	MET
	atmg00480	ATP8, encodes subunit 8 of the mitochondrial F(O) ATP synthase complex	0.3	1.5*	MET
	atmg01190	ATP1, ATPase subunit 1	0.3	1.2*	MET
	atmg00640	ORF25, encodes a plant b subunit of mitochondrial ATP synthase	0.3	1.3*	MET
	atmg00160	COX2, cytochrome c oxidase subunit 2	0.2	1.5*	MET
	atmg00730	COX3, encodes cytochrome c oxidase subunit 3	0.0	1.1*	MET
	at1g69750	ATCOX19-2, cox19 family protein	0.2	1.3*	MET
	at1g64710	Alcohol dehydrogenase, putative	0.1	1.5*	Alcohol dehydrogenases
	at4g28390	AAC3, ADP/ATP CARRIER3	0.1	1.2*	Transport metabolite transporters
ATP related	at1g02530	PGP12, P-GLYCOPROTEIN12; ATPase	4.7	5.9	ABC transporters and MRS
	at3g47780	ATATH6; ATPase	2.1	4.6	ABC transporters and MRS
	at2g47000	ABCB4, ATP BINDING CASSETTE SUBFAMILY B4	2.1	3.7	ABC transporters and MRS
	at5g47240	atnudt8, *Arabidopsis thaliana* Nudix hydrolase homolog 8	1.3	1.6	Nucleotide metabolism Salvage
	at2g18190	AAA-type ATPase family protein	1.4	2.7	Protein degradation
	at1g57990	ATPUP18; purine transmembrane transporter	1.4	3.7	Transport nucleotides
	at1g68840	RAV2, REGULATOR OF THE ATPASE OF THE VACUOLAR MEMBRANE	1.1	2.2	RNA regulation of transcription
Mitochondrial stress markers[a]	at4g37370	CYP81D8, electron carrier	4.6	4.7	Misc. cytochrome P450
	at5g40690	Unknown	2.9	3.9	Unknown
	at2g41730	Unknown	2.8	4.1	Unknown
	at3g50930	BCS1, CYTOCHROME BC1 SYNTHESIS	3.3	4.2	Protein degradation
	at1g19020	Unknown	1.2	3.7	Unknown
	at2g21640	Unknown, UPOX	1.1	2.8	Unknown
	at1g05340	Unknown	0.2	4.0	Unknown
	at1g57630	Disease resistance protein (TIR class), putative	0.3	4.3	Stress, Biotic, PR proteins
	at4g17340	Tonoplast intrinsic protein TIP2;2	−0.3	−1.6	Transport, major intrinsic proteins, TIP

Genes were extracted from the list of genes exhibiting significant changes in expression upon oligomycin treatment. Average transcript levels were calculated from three independent replicates of Affymetrix AtH1 GeneChips per time point and treatment. Fold changes were calculated from the normalized gene expression data of oligomycin-treated to ethanol control at 1 and 4 h after start of treatment and expressed as $\log_2$. The metabolic annotation data were extracted from ROBIN software. *, Specifically after 4 h; LDH, lactate dehydrogenase; MET, mitochondrial electron transport; MRS, multidrug resistance systems.

[a]Marker genes for oxidative stress and mitochondrial dysfunction according to Gadjev et al. (2006) and Schwarzländer et al. (2012), respectively.

lines compared with controls (Figure 6). Under photorespiratory conditions, the conversion of Gly to Ser is considered the main source of NADH in leaf mitochondria and puts high demands on the respiratory chain as an electron sink (Douce et al., 2001). High NADH concentrations in the matrix (i.e., a high redox state of the matrix NAD pool) also influence Gly decarboxylase activity (reviewed in Douce et al., 2001; Bauwe et al., 2010). An estimated 25 to 50% of reductant is exported to the cytosol during photorespiration (Hanning and Heldt, 1993; Krömer, 1995), possibly to maintain the matrix redox status at acceptable levels. Interestingly, mutants in *Aox1a* also show an accumulation of Gly, suggesting that the loss of this non-proton-pumping respiratory enzyme limits photorespiration (Giraud et al., 2008). In addition, an *Arabidopsis* mutant deficient in the expression of the uncoupling protein UCP1, which is an integral component of the inner mitochondrial membrane able to decrease the proton gradient, is also deficient in photorespiration (Sweetlove et al., 2006). Thus, the above-mentioned upregulation of AOX could help to dissipate high levels of reducing equivalents; however, this may not be sufficient to ensure full Gly decarboxylase activity in δRNAi lines. Alternatively, extramitochondrial sinks for reductant could be overloaded in δRNAi lines, as suggested for CMSII, which shows a slower oxidation of Gly in isolated mitochondria compared with the wild type (Sabar et al., 2000; Dutilleul et al., 2005). However, an important difference is that CMSII plants do not exhibit high Gly-to-Ser ratios, whereas this is the case in Dex-treated δRNAi1 and δRNAi2 lines, which show a respective Gly/Ser of 0.54 (±0.09) and 0.55 (±0.12) compared with 0.21 (±0.09) in the empty vector control (calculated from absolute values based on standard calibration curves), indicating that Gly most likely accumulates due to an acute inhibition of Gly decarboxylase in the matrix.

Plants containing low ATP synthase amounts also showed retarded growth but without any changes in the cellular ATP/ADP ratio (Figure 5). This is surprising since at the end of the night, cellular ATP is mainly derived from mitochondria. Again, similar results are seen in CMSII mutants where leaf extracts and protoplasts contained even higher total ATP levels compared with the wild type at the end of the dark period (Szal et al., 2008). Higher ATP concentrations were also measured in slow growing plants carrying antisense constructs for the ATP synthase subunits gamma and ATP5 (Robison et al., 2009). ATP and ADP levels in δRNAi lines were largely unchanged in our study and resulted in an unchanged ATP/ADP ratio. The increase in Ala (and GABA in short-day-grown plants) in δRNAi lines could point toward an increase in glycolysis that may in part substitute for some of the ATP produced. More likely, the adenylate content is altered by compensatory reactions catalyzed by the adenylate kinase. One established physiological role of the adenylate kinase is the provision of ADP for the ATP synthase (Roberts et al., 1997; Igamberdiev and Kleczkowski, 2006). Apart from that, it has been shown by ^{31}P-nuclear magnetic resonance on isolated mitochondria that in the absence of respiratory substrates and O_2 consumption the adenylate kinase can convert added ADP rapidly to ATP and AMP, thus equilibrating the different adenylates (Roberts et al., 1997). Alternatively, the adenylates in the induced δRNAi lines could be derived from nucleoside diphosphate kinases that can interconvert the different nucleoside di- and triphosphates (Sweetlove et al., 2001).

Taken together, there is increasing evidence that a disturbance of respiratory enzymes and the associated metabolic adjustments influence the development of male and female reproductive tissues. The ATP synthase may play a critical role in meeting the high energy demands to keep the metabolic status in vegetative tissues and most likely also gametophytes.

Successive Upregulation of Alternative Non-Proton-Pumping Respiratory Pathways after Mitochondrial ATP Synthase Inhibition

Having established the metabolic status of a long-term disturbance in ATP synthase, we aimed to unravel the early effects of an ATP synthase inhibition using oligomycin. The inhibitor treatment reduced the cellular ATP/ADP ratio by half within 1 h in whole-plant tissues from seedling liquid cultures (Figure 7). A global transcript analysis was performed after 1 and 4 h, which revealed prominent changes in alternative, non-proton-pumping respiratory pathways.

Apart from several *AOX* genes, *Arabidopsis* contains homologs for alternative, non-proton-pumping NAD(P)H dehydrogenases (Rasmusson et al., 2004). The proteins NDA1, NDA2, and NDC1 localize to the inner side, whereas NDB1, NDB2, and NDB4 localize to the outer side of the inner mitochondrial membrane (Elhafez et al., 2006). Together with the AOX, these alternative respiratory enzymes can create an electron transport chain that enables plants to oxidize large amounts of reductant without concomitant proton pumping (Rasmusson et al., 2004). Transcripts for *AOX1a*, *AOX1d*, and the matrix-facing *NDA1* increased strongly already after 1 h of oligomycin treatment (Table 1, Figure 9C). This may signify an early response to an elevated proton motive force across the inner mitochondrial membrane caused by inhibition of the ATP synthase. After 4 h, *AOX1b*, *NDA2*, and the external *NDB2* and *NDB4*, both of which specifically oxidize NADH when expressed in *Escherichia coli* (Geisler et al., 2007), were strongly upregulated (Table 1). These results are in line with the above-mentioned increase in AOX and the higher Gly/Ser ratio observed in the induced δRNAi lines compared with controls. The upregulation of transcripts for internal and external NADH dehydrogenases seen upon oligomycin treatment strengthens the hypothesis that there is an increased need for oxidation of reductant on both sides of the inner membrane if the ATP synthase is disturbed. This ensures $NAD(P)^+$ regeneration both in matrix and cytosol for other biochemical reactions, as previously suggested (Fernie et al., 2004; Rasmusson et al., 2004; Clifton et al., 2005; Escobar et al., 2006), and seems to be both a short- and a long-term response to disturbances of the ATP synthase.

Metabolic Reprogramming in Oligomycin-Treated Seedlings Suggests Operation of Noncyclic TCA Cycle Activities

Short-term treatment by oligomycin resulted in a decrease in TCA cycle organic acids (citrate and succinate) and several TCA cycle–derived amino acids, especially Gln, Asp, and Asn. By contrast, glycolytic end products, such as pyruvate, lactate, and

Ala, were strongly increased (Figure 8). A reduction of TCA cycle activities was further corroborated by a significant decrease in CO_2 release when oligomycin-treated seedlings were fed ^{14}C3:4-labeled Glc (Figure 7). Highly similar results are observed after inhibition of complex I by rotenone in cell suspension cultures, including a slowdown of the TCA cycle, an accumulation of glycolytic end products, and an upregulation of alternative pathways (Garmier et al., 2008). The observed metabolite changes by rotenone could neither be attributed to a decrease in specific enzyme activities nor to global oxidative stress as shown by ascorbate and glutathione measurements. It was therefore suggested that changes in the steady state levels of reductant could feed back on TCA cycle activities to cause these broad responses (Garmier et al., 2008). As nearly all TCA cycle enzymes are sensitive to high NADH levels (Araújo et al., 2012; reviewed in Noctor et al., 2007), this is also the most likely scenario for the effects seen by oligomycin.

In contrast with a general decrease in TCA cycle intermediates, a strong increase in fumarate was observed (Figure 8). Fumarate has recently been associated with a variety of functions in both plants and non-plant systems (Araújo et al., 2011), including as an alternative carbon sink for photosynthate (Pracharoenwattana et al., 2010; Zell et al., 2010). Fumarate can be derived from three metabolic reactions: (1) from succinate via succinate dehydrogenase; (2) from phospho*enol*pyruvate decarboxylation via oxaloacetate, which can feed into the TCA cycle to produce malate and fumarate, thereby exporting reductant (Hanning and Heldt, 1993); and (3) by conversion from malate by the cytosolic fumarase, which is suggested to be of functional relevance particularly during growth on high nitrogen (Pracharoenwattana et al., 2010; Zell et al., 2010). The fumarate accumulation observed in our experiments could be the result of a reallocation of excess carbon and reductant that cannot be used for biosynthetic reactions due to ATP deprivation by employing mechanism (2) or (3). In agreement with this, fumarate depletion is commonly observed under conditions of carbon starvation, during which it is regarded as an important respiratory substrate (Gibon et al., 2009).

Several glycolysis-derived amino acids and glycolytic end products were strongly upregulated in oligomycin-treated seedlings (Figures 7 and 8). The increase in lactate suggests a switch to fermentation, which is likely to occur in response to the observed decrease in TCA cycle activity. Similar responses have been observed during hypoxia induced by water logging of *Lotus japonicus* (Rocha et al., 2010). Additionally, increased GABA levels suggest activation of the GABA shunt, a well-known bypass of the TCA cycle, which carries a great flux of carbon and is a considerable alternative source of succinate (Fait et al., 2008). Taken together, the increases in fumarate and GABA suggest noncyclic TCA activities, possibly to increase carbon storage.

Signaling of ATP Synthase Dysfunction

Mitochondrial retrograde signaling for the maintenance of redox homeostasis has been researched extensively in recent years; however, whole pathways have not been identified (Rhoads and Subbaiah, 2007). A recent meta-analysis of microarray data from stable mutants and short-term chemical treatments revealed protein synthesis, photosynthetic light reactions, and plant–pathogen interactions as three main functional targets of mitochondrial retrograde signaling (Schwarzländer et al., 2012). The data for ATP synthase deficiencies included oligomycin responses of light-grown suspension cultures (Clifton et al., 2005), tobacco (*Nicotiana tabacum*) suspension cultures (Wakamatsu et al., 2010), and whole flower tissue of transgenic plants (*u-ATP9*) that express the unedited form of ATP synthase subunit 9 specifically in flowers (Busi et al., 2011). Except for the flower study, the observed transcript changes show considerable overlaps with the oligomycin results from our study and the changes caused by complex I dysfunction, in particular regarding biotic defense responses (Schwarzländer et al., 2012). Indeed, a high tolerance to ozone, tobacco mosaic virus, and moderate stresses was observed in complex I mutants (Dutilleul et al., 2003b; Meyer et al., 2009).

As presented in Figure 9, the MapMan bins for mitochondrial electron transport/ATP synthesis and hormone metabolism show an early significant increase after oligomycin treatment before a broad transcriptional reprogramming is seen after 4 h. A large portion of the genes upregulated after 1 h are overrepresented in specific clusters that are closely connected in the meta-network coexpression tool AraGenNet (http://aranet.mpimp-golm.mpg.de/aranet/AraGenNet; Mutwil et al., 2010). This means that many of the upregulated genes have similar expression profiles over a range of environmental and developmental conditions. For example, 31 of the 102 oligomycin-induced genes are associated with cluster 58. This cluster is enriched with terms for mitochondrial electron transport and ATP synthesis. In addition, both cluster 58 and neighboring clusters, which also hold many genes that were upregulated in response to oligomycin, contain a large number of biotic stress–related genes. For instance, several of the upregulated transcription factors, such as WRKY70, WRKY25, and WRKY33, have been suggested as candidates central to the activation of defense programs (Eulgem and Somssich, 2007) and may regulate aspects of plant development connected with redox signaling events.

In summary, three independent approaches were taken in this study to analyze the responses of plants to a deficiency in ATP synthase and how these changes influence growth and development. The short-term inhibition of the ATP synthase by oligomycin led to a gradual decrease in the cellular ATP/ADP ratio and a transcriptional reprogramming consisting of an early and massive induction of alternative respiratory pathways. The metabolite profiles suggest a disconnection between glycolysis, the TCA cycle, and the electron transport chain, most likely due to a change in matrix reduction state. The later transcript changes affected hormone metabolism and transcription factors and indicate the initiation of developmental changes. Upregulation of alternative pathways seems to be a common response to ATP synthase deficiencies, and other respiratory defects, since it was also observed in δRNAi plants that held reduced amounts of ATP synthase. These plants showed severe growth retardations but did not suffer from lack of ATP since the ATP/ADP ratio remained unchanged. However, changes were seen in steady state levels of specific primary metabolites, mainly Gly

and Ala. These results strongly indicate that the retarded growth in δRNAi seedlings is rather linked to the metabolic adjustments and not a direct consequence of energy deficiency. More specifically, and supported by the oligomycin study, the need to maintain energy homeostasis could bring about the long-term metabolic changes that then result in delayed growth. Finally, the decreased fertility of the δRNAi plants and of the T-DNA insertion line *atpδ-1* indicates that the above-mentioned adjustments during vegetative growth may fail during high energy demands (e.g., during flower or pollen development).

Gametophyte development is very well studied on the genetic level. Our results, together with other recent reports, strongly suggest that this knowledge needs to be expanded and connected with the regulation of development by metabolic control. Broad metabolic and transcript changes were seen in male sterile flowers with a specific mitochondrial dysfunction (Busi et al., 2011). As an example for nonmitochondrial defects, mutations in the plastidial glyceraldehyde-3-phosphate dehydrogenase alter the development of the tapetum and also lead to male sterility (Muñoz-Bertomeu et al., 2010). While the exact signaling cascades linking changes in ATP/ADP ratios to primary metabolism and development during vegetative and reproductive stages still remain to be unraveled, here, we discover several links between metabolic regulation and gametophyte development. From these results, redox regulation, hormone responses, and plant defense mechanisms represent clear targets for future research.

METHODS

T-DNA Insertion Lines, Pollen Tube Growth, and Ovule Preparations

Seeds of the *Arabidopsis thaliana* accession Columbia-0 (Col-0) as well as the At5g47030 mutant seeds (SAIL_205_C06, SAIL_3_F04, and SAIL_346_G06) were obtained from the Nottingham Arabidopsis Seed Stock Centre. The T-DNA insertion lines were first screened for the insertion by spraying with BASTA (Sanofi-Aventis). Genomic DNA from leaves of resistant plants was then analyzed by PCR using the primers in Supplemental Table 3.1 online, and the sites of T-DNA insertion were verified by sequencing the PCR products. Pollen tube growth was analyzed according to Li et al. (1999) and imaged with a fluorescence microscope (Olympus Bx-51). Ovules were dissected from premature pistils and prepared and analyzed according to Schneitz et al. (1995).

Vector Construction and Transformation

For complementation, the delta gene was amplified from genomic DNA including a 1-kb fragment upstream of the start codon using the primers in Supplemental Table 3.2 online and ligated into the pCAMBIA1390 vector (Cambia). The constructs were verified by sequencing and transformed into heterozygous SAIL_205_C06 (*atpδ-1*) plants via an *Agrobacterium tumefaciens*–mediated transformation protocol (Mersereau et al., 1990) and screened by BASTA and PCR.

For RNAi constructs, the fragment 1 to 267 bp of the delta cDNA sequence was amplified with primers for the sense and antisense direction as described in Supplemental Table 3.3 online and cloned into the vector pUC-RNAi. The sense-antisense fragment was subcloned via restriction digestion using *Pac*I and *Asc*I into the pV-TOP vector, which was previously modified to contain these restriction sites in the multiple cloning cassette between the cauliflower mosaic virus 35S minimal promoter and the ocs terminator. After sequence verification, the RNAi construct and the empty pV-TOP vector were transformed into the *Arabidopsis* activator line 4c-S7, and plants were selected and maintained as described (Craft et al., 2005).

qRT-PCR

Total RNA isolation and cDNA synthesis were done as described by Escobar et al. (2006), using the RNeasy plant mini kit (Qiagen) and SuperScript III reverse transcriptase (Invitrogen). Contamination of genomic DNA was degraded with the Turbo DNA free kit (Ambion). qRT-PCR was performed with transcripts of *GLYCERALDEHYDE-3-PHOSPHATE DEHYDROGENASE* (*GAPDH*) and *UBIQUITIN10* (*UBQ10*) as controls (see Supplemental Table 3.4 online). Fluorescence data were analyzed using SDS 2.3 software (Applied Biosystems), and PCR efficiencies were calculated using LinregPCR software (Ramakers et al., 2003). To compare the gene expression, cycle threshold (C_T) values for all samples were normalized to the C_T value of GAPDH. Expression data were compared using the following formulae: $\Delta C_T = C_{T\ HKG} - C_{T\ GOI}$; $REL_{GOI} = E^{\Delta C_T}$; $REL = REL_{GOI}/REL_{WT}$. C_T is the PCR cycle number at which a set threshold value (0.1) of SYBRGreen fluorescence is reached, ΔC_T is the normalized C_T value of gene of interest (GOI) to the housekeeping gene (HKG), and E is the PCR efficiency which is used to calculate the relative gene expression level (REL_{GOI}) of different samples.

Plant Material, Growth Conditions, and Treatments

For plate-grown seedlings, seeds were surface sterilized, plated on half-strength MS medium (Duchefa), solidified with 0.7% agar and supplements as indicated, and stratified overnight. Seedlings were grown in climate chambers under long-day conditions, 16-h day (120 μmol m^{-2} s^{-1}, 22°C) and 8-h night (22°C), or short-day conditions, 8-h day (22°C) and 16-h night (20°C).

For plants on soil, seeds were first germinated on plates, seedlings were then transferred to soil after 10 d and grown in the greenhouse under long-day conditions (16 h light; 200 μmol m^{-2} s^{-1}) at 50 to 80% relative humidity (20°C) in the day and 50% relative humidity (18°C) in the night. In summer, the lamps were on from 6 AM until 10 AM and from 6 PM until 10 PM.

Seedling liquid cultures used for BN-PAGE analyses and oligomycin treatments were grown as described by Sweetlove et al. (2007) but without agar in the medium. Ten milligrams of seeds (~100 seeds) was inoculated into 80 mL of medium in 250 mL flask. Seedlings were grown at 60 rpm under a 16-h-day/8-h-night cycle. Batches of seedlings were washed with water and dried using a mild centrifugation and blotting on filter paper. The seedlings were used for mitochondrial isolation immediately after harvesting or frozen in liquid nitrogen and stored in −80°C for other experiments. The frozen materials were ground in a ball-mill precooled with liquid nitrogen.

Oligomycin (Sigma-Aldrich) was dissolved at 10 mM ethanol as stock solution and stored at −20°C. For treatments, 80 μL of the stock was added to the seedling cultures for a final concentration of 10 μM, and an equal volume of ethanol was used as control. For Dex treatments, Dex (Sigma-Aldrich) was dissolved at 100 mM DMSO as stock solution and kept at −20°C (Craft et al., 2005). For treatment of leaves, 20 μM Dex in water solution in a volume of 5 mL containing 1 μL Silwet L-77 (Newman Agrochemicals), a surfactant to reduce the surface tension of the solution, was used. The solution was directly applied on the upper and lower side of leaves using a small brush. Control plants were treated with a DMSO in water solution containing Silwet.

Mitochondrial Purification, PAGE Analysis, and Spot Identification

Mitochondria were isolated from ~30 g of seedlings in five flasks of culture as described by Sweetlove et al. (2007). Each biological replicate came from cultures grown and harvested at different times. Protein

content of a mitochondrial preparation was determined using Bio-Rad protein assay kit. Mitochondria to give 200 and 500 μg of protein were used for one-dimensional and two-dimensional BN-PAGE analysis, respectively.

BN-PAGE was performed according to Obata et al. (2011). Mitochondria were resuspended in solubilization buffer (30 mM HEPES-KOH, pH 7.0, 150 mM potassium acetate, 10% [w/v] glycerol, and 5% digitonin) to give 5 μg protein per mL. The solution was kept on ice for 20 min, and samples were then centrifuged at 18,000*g* for 20 min to remove insoluble constituents. After adding 5% volume of a 5% (w/v) Coomassie Brilliant Blue solution to the supernatant, the samples were loaded onto 4.5 to 12% (w/v) acrylamide gradient gels. For two-dimensional BN-PAGE analysis, gel lanes were cut out and incubated with reduction buffer (2% SDS, 66 mM Na_2CO_3, and 2% β-mercaptoethanol) for 1 h at room temperature. Separation in the second dimension was performed with 12.5% acrylamide gel containing 4 M urea. Gels were stained with Coomassie Brilliant Blue G 250 by blue-silver staining (Candiano et al., 2004). The image was scanned by the Odyssey system (Li-COR). For spot identification, protein spots were excised from the gel and subjected to tryptic digestion followed by liquid chromatography–tandem mass spectrometry analysis as described by Obata et al. (2011).

RNA in Situ Hybridization and Histochemical GUS Analysis

RNA in situ hybridization was essentially performed as previously described (Weigel and Glazebrook, 2002). Inflorescences of Col-0 were paraffin embedded using an ASP300S embedding automat (Leica) and an EG1160 tissue embedding station (Leica). Sections (8 to 10 μm) were prepared on a RM2265 rotary microtome (Leica). For RNA probe synthesis, the delta gene (At5g47030) was amplified with primers shown in Supplemental Table 3.2 online and cloned into a pCRII-TOPO Dual Promoter vector (Invitrogen). RNA probe synthesis was performed with the DIG RNA labeling kit (Roche Applied Science) according to the manufacturer's instructions. Sections were imaged with a BX61 microscope (Olympus) equipped with differential interference contrast, using a ×10 objective and a Colorview III digital camera (Olympus) controlled with the cell^P software from Olympus. Sense probes did not result in any noticeable staining.

For histochemical GUS analyses, a 1078-bp fragment from the delta promoter region was amplified from Col-0 genomic DNA using the primers listed in Supplemental Table 3.5 online and ligated into pCAMBIA 1305.2 (Cambia). The verified constructs were transformed into *Arabidopsis* (Col-0 ecotype) and screened for positive transformants. The GUS staining was performed according to Jefferson et al. (1987).

Transmission Electron Microscopy

Freshly harvested flowers of *Arabidopsis* mutants and the wild type were transferred to the fixative solution mixture of 2.5% glutaraldehyde and 2% paraformaldehyde in 0.2 M cacodylate buffer, pH 7.4, for a minimum of 4 h at room temperature. Postfixation was done in 1% OsO_4 in the same buffer for 2 h. The tissues were dehydrated in a series of ethanol and propylene oxide and embedded in Spurr's low viscosity epoxy resin (Spurr, 1969). Ultrathin sections (60 to 70 nm) were cut on a Leica UC6 ultramicrotome using a diamond knife, stained with uranyl acetate and lead citrate (Reynolds, 1963), and examined on a Zeiss energy filtering transmission electron microscope at 80 kV.

Environmental Scanning Electron Microscopy

Pollen from *Arabidopsis* flowers was fixed on the sample holder of the Quanta 600 FEG environmental scanning electron microscope (FEI Europe) and investigated under low vacuum mode conditions to minimize drying processes of the samples under the following settings: temperature 5°C, pressure 1 Torr, and voltage 5 kV.

Determination of Adenylate and Metabolite Levels

Green tissue from plate-grown seedlings or whole liquid cultures was sampled at the indicated time points, immediately frozen in liquid nitrogen, and stored at −80°C until further analysis. Extraction was performed by grinding the frozen materials in a ball-mill precooled with liquid nitrogen and immediate addition of the appropriate extraction buffers. For adenylate analyses, trichloroacetic acid extracts were prepared according to Jelitto et al. (1992). UDP-Glc, ATP, and ADP in trichloroacetic acid extracts were measured by HPLC, using a Bio-Tek HPLC system (pump-system 522, HPLC autosampler 560, HPLC 535 UV detector) with a Partisil-SAX anion exchange column (10 μm; Knauer) with ammonium dihydrogen phosphate buffers (Merck) according to Geigenberger et al. (1997). Data analysis was performed with chromeleon 6.80 software (Dionex).

For GC-MS, the plant metabolites were extracted and analyzed as described previously (Lisec et al., 2006). Metabolites were identified in comparison to database entries of authentic standards (Kopka et al., 2005; Schauer et al., 2005).

Measurement of Respiratory Parameters

Estimations of the TCA cycle flux on the basis of $^{14}CO_2$ evolution were performed following incubation of liquid seedling cultures in 10 mM MES-KOH, pH 6.5, containing 2.32 KBq mL^{-1} of [1-^{14}C]-, [2-^{14}C]-,[3,4-^{14}C]-, or [6-^{14}C]Glc as done by Nunes-Nesi et al. (2005). $^{14}CO_2$ evolved was trapped in KOH and quantified by liquid scintillation counting. The results were interpreted following Rees and Beevers (1960). Radiolabeled D-[1-^{14}C]-, D-[2-^{14}C]Glc D-[3:4-^{14}C]-, and D-[6-^{14}C]Glc were from American Radiolabeled Chemicals.

Respiration rates in whole tissues were determined by measuring the O_2 concentration in the incubation medium at 25°C using a Fibox-3 optical oxygen sensor (PreSens). Approximately 10 mg tissue (fresh weight) was transferred into the vessel containing 1 mL MS medium including 30 mM Suc. Oxygen uptake was measured in the dark immediately after transferring the seedlings to the reaction vessel, 5 min after the addition of KCN (1 mM), and again 5 min after the addition of *n*-propyl gallate (0.1 mM), with reoxygenation of the medium during inhibitor incubations. Capacity of AOX was calculated as the rate with KCN minus the rate with KCN and *n*-propyl gallate (Escobar et al., 2006). For flower tissue, salicylhydroxamic acid (1 mM final concentration) was used instead of *n*-propyl gallate as AOX inhibitor since the latter was not fully inhibiting the activities, presumably due to the activation of KCN-sensitive peroxidases (Møller et al., 1988). The total respiration rate was calculated as the total O_2 consumption minus the rate in the presence of both inhibitors (<10% of the total).

Microarray Analysis

RNA was extracted as described above and labeled with the MessageAmp II-Biotin Enhanced kit (Ambion). After verifying RNA integrity by the Agilent RNA 6000 Nano Kit and the Agilent 2100 Bioanalyzer, the labeled aRNA was hybridized to Affymetrix ATH1 Genome arrays at ATLAS Biolabs. Hybridizations were done on three biological replicates (i.e., three culture flasks, per time point and treatment). The data were analyzed using Robin (Lohse et al., 2010) with the default settings of RMA (robust multi array averaging) and $P < 0.05$ and visualized with MapMan (Thimm et al., 2004) and PageMan (Usadel et al., 2009).

Statistical Analysis

Data were statistically examined using analysis of variance and tested for significant ($P < 0.05$) differences using Student's *t* tests. The term significant is used in the text only when the change in question has been confirmed to be significant ($P < 0.05$) with the Student's *t* test. All the

statistical analyses were performed using the algorithm embedded into Microsoft Excel.

Accession Numbers

Sequence data from this article can be found in the Arabidopsis Genome Initiative or GenBank/EMBL databases under the following accession numbers: ATPδ, At5g47030, GAPDH, At1g13440; and UBQ10, At4g05320. Expression data from this article can be found in the NCBI database (http://www.ncbi.nlm.nih.gov/) under the accession number GSE38965.

Supplemental Data

The following materials are available in the online version of this article.

Supplemental Figure 1. Pollen and Tapetum Morphology in Heterozygous *atp*δ*-1* and the Wild Type Imaged by Transmission Electron Microscopy.

Supplemental Figure 2. Delta Transcript and Adenylates in δRNAi Lines Grown under Different Conditions.

Supplemental Figure 3. Growth of δRNAi Lines in Different Light Regimes and Sugar Conditions.

Supplemental Figure 4. AOX Capacity of δRNAi Lines and Controls in Different Tissues.

Supplemental Figure 5. Adenylate and Metabolite Levels in Oligomycin-Treated Seedlings.

Supplemental Table 1. Complementation of *atp*δ*-1* Shown by BASTA Resistance.

Supplemental Table 2. Selected Transcripts Induced by Oligomycin after 1 and 4 h Grouped into Functional Classes.

Supplemental Table 3. Primers Used in the Experiments.

Supplemental Data Set 1. LC-MS Analyses of Spots from 2D Gels.

Supplemental Data Set 2. Overview of the Metabolite Reporting List.

ACKNOWLEDGMENTS

We thank Allan G. Rasmusson for critical reading of the article, Joost van Dongen and David M. Mueller for valuable discussions, Heike Riegler for help with the HPLC, Ilse Balbo for help with GC-MS, Colin Rupprecht and Anja Fröhlich for assistance with in situ hybridizations, and Ian Moore for providing the pV-TOP vector system. D.A.G., C.P., and S.P. were funded by the Max-Planck-Gesellschaft.

AUTHOR CONTRIBUTIONS

D.A.G., C.P, A.R.F., and S.P. designed the research, performed research, analyzed data, and wrote the article. T.O., A.N.-N., A.M., K.S., E.M., and W.L.A. designed the research, performed the research, and analyzed data.

Received April 12, 2012; revised June 20, 2012; accepted June 27, 2012; published July 17, 2012.

REFERENCES

Araújo, W.L., Nunes-Nesi, A., and Fernie, A.R. (2011). Fumarate: Multiple functions of a simple metabolite. Phytochemistry **72:** 838–843.

Araújo, W.L., Nunes-Nesi, A., Nikoloski, Z., Sweetlove, L.J., and Fernie, A.R. (2012). Metabolic control and regulation of the tricarboxylic acid cycle in photosynthetic and heterotrophic plant tissues. Plant Cell Environ. **35:** 1–21.

Arnold, I., Pfeiffer, K., Neupert, W., Stuart, R.A., and Schägger, H. (1998). Yeast mitochondrial F_1F_0-ATP synthase exists as a dimer: Identification of three dimer-specific subunits. EMBO J. **17:** 7170–7178.

Bauwe, H., Hagemann, M., and Fernie, A.R. (2010). Photorespiration: Players, partners and origin. Trends Plant Sci. **15:** 330–336.

Bergman, P., Edqvist, J., Farbos, I., and Glimelius, K. (2000). Male-sterile tobacco displays abnormal mitochondrial atp1 transcript accumulation and reduced floral ATP/ADP ratio. Plant Mol. Biol. **42:** 531–544.

Busi, M.V., Gomez-Lobato, M.E., Rius, S.P., Turowski, V.R., Casati, P., Zabaleta, E.J., Gomez-Casati, D.F., and Araya, A. (2011). Effect of mitochondrial dysfunction on carbon metabolism and gene expression in flower tissues of *Arabidopsis thaliana*. Mol. Plant **4:** 127–143.

Candiano, G., Bruschi, M., Musante, L., Santucci, L., Ghiggeri, G.M., Carnemolla, B., Orecchia, P., Zardi, L., and Righetti, P.G. (2004). Blue silver: A very sensitive colloidal Coomassie G-250 staining for proteome analysis. Electrophoresis **25:** 1327–1333.

Carlsson, J., Leino, M., Sohlberg, J., Sundström, J.F., and Glimelius, K. (2008). Mitochondrial regulation of flower development. Mitochondrion **8:** 74–86.

Clifton, R., Lister, R., Parker, K.L., Sappl, P.G., Elhafez, D., Millar, A.H., Day, D.A., and Whelan, J. (2005). Stress-induced co-expression of alternative respiratory chain components in *Arabidopsis thaliana*. Plant Mol. Biol. **58:** 193–212.

Craft, J., Samalova, M., Baroux, C., Townley, H., Martinez, A., Jepson, I., Tsiantis, M., and Moore, I. (2005). New pOp/LhG4 vectors for stringent glucocorticoid-dependent transgene expression in *Arabidopsis*. Plant J. **41:** 899–918.

Douce, R., Bourguignon, J., Neuburger, M., and Rébeillé, F. (2001). The glycine decarboxylase system: A fascinating complex. Trends Plant Sci. **6:** 167–176.

Dudkina, N.V., Heinemeyer, J., Keegstra, W., Boekema, E.J., and Braun, H.P. (2005). Structure of dimeric ATP synthase from mitochondria: An angular association of monomers induces the strong curvature of the inner membrane. FEBS Lett. **579:** 5769–5772.

Dudkina, N.V., Oostergetel, G.T., Lewejohann, D., Braun, H.P., and Boekema, E.J. (2010). Row-like organization of ATP synthase in intact mitochondria determined by cryo-electron tomography. Biochim. Biophys. Acta **1797:** 272–277.

Dutilleul, C., Driscoll, S., Cornic, G., De Paepe, R., Foyer, C.H., and Noctor, G. (2003a). Functional mitochondrial complex I is required by tobacco leaves for optimal photosynthetic performance in photorespiratory conditions and during transients. Plant Physiol. **131:** 264–275.

Dutilleul, C., Garmier, M., Noctor, G., Mathieu, C., Chétrit, P., Foyer, C.H., and de Paepe, R. (2003b). Leaf mitochondria modulate whole cell redox homeostasis, set antioxidant capacity, and determine stress resistance through altered signaling and diurnal regulation. Plant Cell **15:** 1212–1226.

Dutilleul, C., Lelarge, C., Prioul, J.L., De Paepe, R., Foyer, C.H., and Noctor, G. (2005). Mitochondria-driven changes in leaf NAD status exert a crucial influence on the control of nitrate assimilation and the integration of carbon and nitrogen metabolism. Plant Physiol. **139:** 64–78.

Duvezin-Caubet, S., Caron, M., Giraud, M.F., Velours, J., and di Rago, J.P. (2003). The two rotor components of yeast mitochondrial ATP synthase are mechanically coupled by subunit δ. Proc. Natl. Acad. Sci. USA **100:** 13235–13240.

Elhafez, D., Murcha, M.W., Clifton, R., Soole, K.L., Day, D.A., and Whelan, J. (2006). Characterization of mitochondrial alternative NAD(P)H dehydrogenases in *Arabidopsis*: Intraorganelle location and expression. Plant Cell Physiol. **47:** 43–54.

Escobar, M.A., Geisler, D.A., and Rasmusson, A.G. (2006). Reorganization of the alternative pathways of the *Arabidopsis* respiratory chain by nitrogen supply: Opposing effects of ammonium and nitrate. Plant J. **45:** 775–788.

Eulgem, T., and Somssich, I.E. (2007). Networks of WRKY transcription factors in defense signaling. Curr. Opin. Plant Biol. **10:** 366–371.

Fait, A., Fromm, H., Walter, D., Galili, G., and Fernie, A.R. (2008). Highway or byway: The metabolic role of the GABA shunt in plants. Trends Plant Sci. **13:** 14–19.

Fernie, A.R., Carrari, F., and Sweetlove, L.J. (2004). Respiratory metabolism: Glycolysis, the TCA cycle and mitochondrial electron transport. Curr. Opin. Plant Biol. **7:** 254–261.

Gadjev, I., Vanderauwera, S., Gechev, T.S., Laloi, C., Minkov, I.N., Shulaev, V., Apel, K., Inzé, D., Mittler, R., and Van Breusegem, F. (2006). Transcriptomic footprints disclose specificity of reactive oxygen species signaling in Arabidopsis. Plant Physiol. **141:** 436–445.

Garmier, M., Carroll, A.J., Delannoy, E., Vallet, C., Day, D.A., Small, I.D., and Millar, A.H. (2008). Complex I dysfunction redirects cellular and mitochondrial metabolism in Arabidopsis. Plant Physiol. **148:** 1324–1341.

Geigenberger, P., Reimholz, R., Geiger, M., Merlo, L., Canale, V., and Stitt, M. (1997). Regulation of sucrose and starch metabolism in potato tubers in response to short-term water deficit. Planta **201:** 502–518.

Geisler, D.A., Broselid, C., Hederstedt, L., and Rasmusson, A.G. (2007). Ca^{2+}-binding and Ca^{2+}-independent respiratory NADH and NADPH dehydrogenases of *Arabidopsis thaliana*. J. Biol. Chem. **282:** 28455–28464.

Gibon, Y., Pyl, E.-T., Sulpice, R., Lunn, J.E., Höhne, M., Günther, M., and Stitt, M. (2009). Adjustment of growth, starch turnover, protein content and central metabolism to a decrease of the carbon supply when *Arabidopsis* is grown in very short photoperiods. Plant Cell Environ. **32:** 859–874.

Giraud, E., Ho, L.H., Clifton, R., Carroll, A., Estavillo, G., Tan, Y.F., Howell, K.A., Ivanova, A., Pogson, B.J., Millar, A.H., and Whelan, J. (2008). The absence of ALTERNATIVE OXIDASE1a in Arabidopsis results in acute sensitivity to combined light and drought stress. Plant Physiol. **147:** 595–610.

Gledhill, J.R., and Walker, J.E. (2006). Inhibitors of the catalytic domain of mitochondrial ATP synthase. Biochem. Soc. Trans. **34:** 989–992.

Gutierres, S., Sabar, M., Lelandais, C., Chetrit, P., Diolez, P., Degand, H., Boutry, M., Vedel, F., de Kouchkovsky, Y., and De Paepe, R. (1997). Lack of mitochondrial and nuclear-encoded subunits of complex I and alteration of the respiratory chain in *Nicotiana sylvestris* mitochondrial deletion mutants. Proc. Natl. Acad. Sci. USA **94:** 3436–3441.

Hanning, I., and Heldt, H.W. (1993). On the function of mitochondrial metabolism during photosynthesis in spinach (*Spinacia oleracea* L.) leaves. Partitioning between respiration and export of redox equivalents and precursors for nitrate assimilation products. Plant Physiol. **103:** 1147–1154.

Hanson, M.R., and Bentolila, S. (2004). Interactions of mitochondrial and nuclear genes that affect male gametophyte development. Plant Cell **16** (suppl.)**:** S154–S169.

Heiser, V., Rasmusson, A.G., Thieck, O., Brennicke, A., and Grohmann, L. (1997). Antisense repression of the mitochondrial NADH-binding subunit of complex I in transgenic potato plants affects male fertility. Plant Sci. **127:** 61–69.

Ho, L.H., Giraud, E., Uggalla, V., Lister, R., Clifton, R., Glen, A., Thirkettle-Watts, D., Van Aken, O., and Whelan, J. (2008). Identification of regulatory pathways controlling gene expression of stress-responsive mitochondrial proteins in Arabidopsis. Plant Physiol. **147:** 1858–1873.

Igamberdiev, A.U., and Kleczkowski, L.A. (2006). Equilibration of adenylates in the mitochondrial intermembrane space maintains respiration and regulates cytosolic metabolism. J. Exp. Bot. **57:** 2133–2141.

Jefferson, R.A., Kavanagh, T.A., and Bevan, M.W. (1987). GUS fusions: Beta-glucuronidase as a sensitive and versatile gene fusion marker in higher plants. EMBO J. **6:** 3901–3907.

Jelitto, T., Sonnewald, U., Willmitzer, L., Hajirezeai, M., and Stitt, M. (1992). Inorganic pyrophosphate content and metabolites in potato and tobacco plants expressing *E. coli* pyrophosphatase in their cytosol. Planta **188:** 238–244.

Kopka, J. et al. (2005). GMD@CSB.DB: The Golm Metabolome Database. Bioinformatics **21:** 1635–1638.

Kovtun, Y., Chiu, W.-L., Tena, G., and Sheen, J. (2000). Functional analysis of oxidative stress-activated mitogen-activated protein kinase cascade in plants. Proc. Natl. Acad. Sci. USA **97:** 2940–2945.

Krömer, S. (1995). Respiration during photosynthesis. Annu. Rev. Plant Physiol. Plant Mol. Biol. **46:** 45–70.

Krömer, S., Stitt, M., and Heldt, H.W. (1988). Mitochondrial oxidative phosphorylation participating in photosynthetic metabolism of a leaf cell. FEBS Lett. **226:** 352–356.

Lai-Zhang, J., Xiao, Y., and Mueller, D.M. (1999). Epistatic interactions of deletion mutants in the genes encoding the F_1-ATPase in yeast *Saccharomyces cerevisiae*. EMBO J. **18:** 58–64.

Landschütze, V., Willmitzer, L., and Müller-Röber, B. (1995). Inhibition of flower formation by antisense repression of mitochondrial citrate synthase in transgenic potato plants leads to a specific disintegration of the ovary tissues of flowers. EMBO J. **14:** 660–666.

Lee, S.-L.J., and Warmke, H.E. (1979). Organelle size and number in fertile and T-cytoplasmic male sterile corn. Am. J. Bot. **66:** 141–148.

León, G., Holuigue, L., and Jordana, X. (2007). Mitochondrial complex II is essential for gametophyte development in Arabidopsis. Plant Physiol. **143:** 1534–1546.

Li, H., Lin, Y., Heath, R.M., Zhu, M.X., and Yang, Z. (1999). Control of pollen tube tip growth by a Rop GTPase-dependent pathway that leads to tip-localized calcium influx. Plant Cell **11:** 1731–1742.

Li, W.Q., Zhang, X.Q., Xia, C., Deng, Y., and Ye, D. (2010). MALE GAMETOPHYTE DEFECTIVE 1, encoding the F_Ad subunit of mitochondrial F_1F_0-ATP synthase, is essential for pollen formation in *Arabidopsis thaliana*. Plant Cell Physiol. **51:** 923–935.

Lisec, J., Schauer, N., Kopka, J., Willmitzer, L., and Fernie, A.R. (2006). Gas chromatography mass spectrometry-based metabolite profiling in plants. Nat. Protoc. **1:** 387–396.

Lohse, M. et al. (2010). Robin: An intuitive wizard application for R-based expression microarray quality assessment and analysis. Plant Physiol. **153:** 642–651.

Lunn, J.E., Feil, R., Hendriks, J.H., Gibon, Y., Morcuende, R., Osuna, D., Scheible, W.R., Carillo, P., Hajirezaei, M.R., and Stitt, M. (2006). Sugar-induced increases in trehalose 6-phosphate are correlated with redox activation of ADPglucose pyrophosphorylase and higher rates of starch synthesis in *Arabidopsis thaliana*. Biochem. J. **397:** 139–148.

Ma, H. (2005). Molecular genetic analyses of microsporogenesis and microgametogenesis in flowering plants. Annu. Rev. Plant Biol. **56:** 393–434.

Maxwell, D.P., Wang, Y., and McIntosh, L. (1999). The alternative oxidase lowers mitochondrial reactive oxygen production in plant cells. Proc. Natl. Acad. Sci. USA **96:** 8271–8276.

Mersereau, M., Pazour, G.J., and Das, A. (1990). Efficient transformation of *Agrobacterium tumefaciens* by electroporation. Gene **90:** 149–151.

Meyer, E.H., Tomaz, T., Carroll, A.J., Estavillo, G., Delannoy, E., Tanz, S.K., Small, I.D., Pogson, B.J., and Millar, A.H. (2009). Remodeled respiration in *ndufs4* with low phosphorylation efficiency suppresses Arabidopsis germination and growth and alters control of metabolism at night. Plant Physiol. **151:** 603–619.

Møller, I.M., Bérczi, A., van der Plas, L.H.W., and Lambers, H. (1988). Measurement of the activity and capacity of the alternative pathway in intact plant tissues: Identification of problems and possible solutions. Physiol. Plant. **72:** 642–649.

Møller, I.M., and Sweetlove, L.J. (2010). ROS signalling—Specificity is required. Trends Plant Sci. **15:** 370–374.

Muñoz-Bertomeu, J., Cascales-Miñana, B., Irles-Segura, A., Mateu, I., Nunes-Nesi, A., Fernie, A.R., Segura, J., and Ros, R. (2010). The plastidial glyceraldehyde-3-phosphate dehydrogenase is critical for viable pollen development in Arabidopsis. Plant Physiol. **152:** 1830–1841.

Mutwil, M., Usadel, B., Schütte, M., Loraine, A., Ebenhöh, O., and Persson, S. (2010). Assembly of an interactive correlation network for the Arabidopsis genome using a novel heuristic clustering algorithm. Plant Physiol. **152:** 29–43.

Noctor, G., De Paepe, R., and Foyer, C.H. (2007). Mitochondrial redox biology and homeostasis in plants. Trends Plant Sci. **12:** 125–134.

Nunes-Nesi, A., Carrari, F., Lytovchenko, A., Smith, A.M., Loureiro, M.E., Ratcliffe, R.G., Sweetlove, L.J., and Fernie, A.R. (2005). Enhanced photosynthetic performance and growth as a consequence of decreasing mitochondrial malate dehydrogenase activity in transgenic tomato plants. Plant Physiol. **137:** 611–622.

Obata, T., Matthes, A., Koszior, S., Lehmann, M., Araújo, W.L., Bock, R., Sweetlove, L.J., and Fernie, A.R. (2011). Alteration of mitochondrial protein complexes in relation to metabolic regulation under short-term oxidative stress in Arabidopsis seedlings. Phytochemistry **72:** 1081–1091.

Pang, Y., Wang, H., Song, W.Q., and Zhu, Y.X. (2010). The cotton ATP synthase δ1 subunit is required to maintain a higher ATP/ADP ratio that facilitates rapid fibre cell elongation. Plant Biol (Stuttg) **12:** 903–909.

Paumard, P., Vaillier, J., Coulary, B., Schaeffer, J., Soubannier, V., Mueller, D.M., Brèthes, D., di Rago, J.P., and Velours, J. (2002). The ATP synthase is involved in generating mitochondrial cristae morphology. EMBO J. **21:** 221–230.

Pracharoenwattana, I., Zhou, W.X., Keech, O., Francisco, P.B., Udomchalothorn, T., Tschoep, H., Stitt, M., Gibon, Y., and Smith, S.M. (2010). *Arabidopsis* has a cytosolic fumarase required for the massive allocation of photosynthate into fumaric acid and for rapid plant growth on high nitrogen. Plant J. **62:** 785–795.

Ramakers, C., Ruijter, J.M., Deprez, R.H., and Moorman, A.F. (2003). Assumption-free analysis of quantitative real-time polymerase chain reaction (PCR) data. Neurosci. Lett. **339:** 62–66.

Rasmusson, A.G., Geisler, D.A., and Møller, I.M. (2008). The multiplicity of dehydrogenases in the electron transport chain of plant mitochondria. Mitochondrion **8:** 47–60.

Rasmusson, A.G., Heiser, V., Zabaleta, E., Brennicke, A., and Grohmann, L. (1998). Physiological, biochemical and molecular aspects of mitochondrial complex I in plants. Biochim. Biophys. Acta **1364:** 101–111.

Rasmusson, A.G., Soole, K.L., and Elthon, T.E. (2004). Alternative NAD(P)H dehydrogenases of plant mitochondria. Annu. Rev. Plant Biol. **55:** 23–39.

Rees, T.A., and Beevers, H. (1960). Pathways of glucose dissimilation in carrot slices. Plant Physiol. **35:** 830–838.

Reynolds, E.S. (1963). The use of lead citrate at high pH as an electron-opaque stain in electron microscopy. J. Cell Biol. **17:** 208–212.

Rhoads, D.M., and Subbaiah, C.C. (2007). Mitochondrial retrograde regulation in plants. Mitochondrion **7:** 177–194.

Roberts, J.K.M., Aubert, S., Gout, E., Bligny, R., and Douce, R. (1997). Cooperation and competition between adenylate kinase, nucleoside diphosphokinase, electron transport, and ATP synthase in plant mitochondria studied by ^{31}P-nuclear magnetic resonance. Plant Physiol. **113:** 191–199.

Robison, M.M., Ling, X., Smid, M.P.L., Zarei, A., and Wolyn, D.J. (2009). Antisense expression of mitochondrial ATP synthase subunits OSCP (ATP5) and γ (ATP3) alters leaf morphology, metabolism and gene expression in *Arabidopsis*. Plant Cell Physiol. **50:** 1840–1850.

Rocha, M., Licausi, F., Araújo, W.L., Nunes-Nesi, A., Sodek, L., Fernie, A.R., and van Dongen, J.T. (2010). Glycolysis and the tricarboxylic acid cycle are linked by alanine aminotransferase during hypoxia induced by waterlogging of *Lotus japonicus*. Plant Physiol. **152:** 1501–1513.

Rossel, J.B., Wilson, P.B., Hussain, D., Woo, N.S., Gordon, M.J., Mewett, O.P., Howell, K.A., Whelan, J., Kazan, K., and Pogson, B.J. (2007). Systemic and intracellular responses to photooxidative stress in *Arabidopsis*. Plant Cell **19:** 4091–4110.

Sabar, M., De Paepe, R., and de Kouchkovsky, Y. (2000). Complex I impairment, respiratory compensations, and photosynthetic decrease in nuclear and mitochondrial male sterile mutants of *Nicotiana sylvestris*. Plant Physiol. **124:** 1239–1250.

Schauer, N., Steinhauser, D., Strelkov, S., Schomburg, D., Allison, G., Moritz, T., Lundgren, K., Roessner-Tunali, U., Forbes, M.G., Willmitzer, L., Fernie, A.R., and Kopka, J. (2005). GC-MS libraries for the rapid identification of metabolites in complex biological samples. FEBS Lett. **579:** 1332–1337.

Schneitz, K., Hülskamp, M., and Pruitt, R.E. (1995). Wild-type ovule development in *Arabidopsis thaliana*: A light microscope study of cleared whole-mount tissue. Plant J. **7:** 731–749.

Schwarzländer, M., König, A.C., Sweetlove, L.J., and Finkemeier, I. (2012). The impact of impaired mitochondrial function on retrograde signalling: A meta-analysis of transcriptomic responses. J. Exp. Bot. **63:** 1735–1750.

Sessions, A. et al. (2002). A high-throughput *Arabidopsis* reverse genetics system. Plant Cell **14:** 2985–2994.

Smyth, D.R., Bowman, J.L., and Meyerowitz, E.M. (1990). Early flower development in *Arabidopsis*. Plant Cell **2:** 755–767.

Spurr, A.R. (1969). A low-viscosity epoxy resin embedding medium for electron microscopy. J. Ultrastruct. Res. **26:** 31–43.

Sweetlove, L.J., Heazlewood, J.L., Herald, V., Holtzapffel, R., Day, D.A., Leaver, C.J., and Millar, A.H. (2002). The impact of oxidative stress on *Arabidopsis* mitochondria. Plant J. **32:** 891–904.

Sweetlove, L.J., Lytovchenko, A., Morgan, M., Nunes-Nesi, A., Taylor, N.L., Baxter, C.J., Eickmeier, I., and Fernie, A.R. (2006). Mitochondrial uncoupling protein is required for efficient photosynthesis. Proc. Natl. Acad. Sci. USA **103:** 19587–19592.

Sweetlove, L.J., Mowday, B., Hebestreit, H.F., Leaver, C.J., and Millar, A.H. (2001). Nucleoside diphosphate kinase III is localized to the inter-membrane space in plant mitochondria. FEBS Lett. **508:** 272–276.

Sweetlove, L.J., Taylor, N.L., and Leaver, C.J. (2007). Isolation of intact, functional mitochondria from the model plant *Arabidopsis thaliana*. Methods Mol. Biol. **372:** 125–136.

Szal, B., Dabrowska, Z., Malmberg, G., Gardeström, P., and Rychter, A.M. (2008). Changes in energy status of leaf cells as

a consequence of mitochondrial genome rearrangement. Planta **227:** 697–706.

Tadege, M., and Kuhlemeier, C. (1997). Aerobic fermentation during tobacco pollen development. Plant Mol. Biol. **35:** 343–354.

Teixeira, R.T., Knorpp, C., and Glimelius, K. (2005). Modified sucrose, starch, and ATP levels in two alloplasmic male-sterile lines of *B. napus*. J. Exp. Bot. **56:** 1245–1253.

Thimm, O., Bläsing, O., Gibon, Y., Nagel, A., Meyer, S., Krüger, P., Selbig, J., Müller, L.A., Rhee, S.Y., and Stitt, M. (2004). MAPMAN: A user-driven tool to display genomics data sets onto diagrams of metabolic pathways and other biological processes. Plant J. **37:** 914–939.

Usadel, B., Poree, F., Nagel, A., Lohse, M., Czedik-Eysenberg, A., and Stitt, M. (2009). A guide to using MapMan to visualize and compare Omics data in plants: A case study in the crop species, maize. Plant Cell Environ. **32:** 1211–1229.

Vanlerberghe, G.C., and McIntosh, L. (1997). Alternative oxidase: From gene to function. Annu. Rev. Plant Physiol. Plant Mol. Biol. **48:** 703–734.

Wakamatsu, K., Fujimoto, M., Nakazono, M., Arimura, S., and Tsutsumi, N. (2010). Fusion of mitochondria in tobacco suspension cultured cells is dependent on the cellular ATP level but not on actin polymerization. Plant Cell Rep. **29:** 1139–1145.

Wang, Z. et al. (2006). Cytoplasmic male sterility of rice with boro II cytoplasm is caused by a cytotoxic peptide and is restored by two related PPR motif genes via distinct modes of mRNA silencing. Plant Cell **18:** 676–687.

Watson, J.M., Fusaro, A.F., Wang, M.B., and Waterhouse, P.M. (2005). RNA silencing platforms in plants. FEBS Lett. **579:** 5982–5987.

Weigel, D., and Glazebrook, J. (2002). Arabidopsis: A Laboratory Manual. (Cold Spring Harbor, NY: Cold Spring Harbor Laboratory Press).

Wilson, Z.A., and Zhang, D.B. (2009). From *Arabidopsis* to rice: Pathways in pollen development. J. Exp. Bot. **60:** 1479–1492.

Xu, P., Zhang, Y.J., Kang, L., Roossinck, M.J., and Mysore, K.S. (2006). Computational estimation and experimental verification of off-target silencing during posttranscriptional gene silencing in plants. Plant Physiol. **142:** 429–440.

Zell, M.B., Fahnenstich, H., Maier, A., Saigo, M., Voznesenskaya, E.V., Edwards, G.E., Andreo, C., Schleifenbaum, F., Zell, C., Drincovich, M.F., and Maurino, V.G. (2010). Analysis of Arabidopsis with highly reduced levels of malate and fumarate sheds light on the role of these organic acids as storage carbon molecules. Plant Physiol. **152:** 1251–1262.